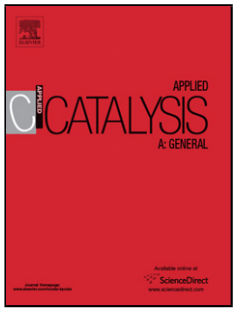

Title: Carbon monoxide hydrogenation on potassium promoted Mo_2N catalysts

Author: Sharif F. Zaman Nagaraju Pasupulety Abdulrahim A. Al-Zahrani Muhammad A. Daous Saad S. Al-Shahrani Hafedh Driss Lachezar A. Petrov Kevin J. Smith

PII: S0926-860X(16)30620-2
DOI: http://dx.doi.org/doi:10.1016/j.apcata.2016.12.015
Reference: APCATA 16100

To appear in: *Applied Catalysis A: General*

Received date: 12-10-2016
Revised date: 12-12-2016
Accepted date: 19-12-2016

Please cite this article as: Sharif F.Zaman, Nagaraju Pasupulety, Abdulrahim A.Al-Zahrani, Muhammad A.Daous, Saad S.Al-Shahrani, Hafedh Driss, Lachezar A.Petrov, Kevin J.Smith, Carbon monoxide hydrogenation on potassium promoted Mo2N catalysts, Applied Catalysis A, General http://dx.doi.org/10.1016/j.apcata.2016.12.015

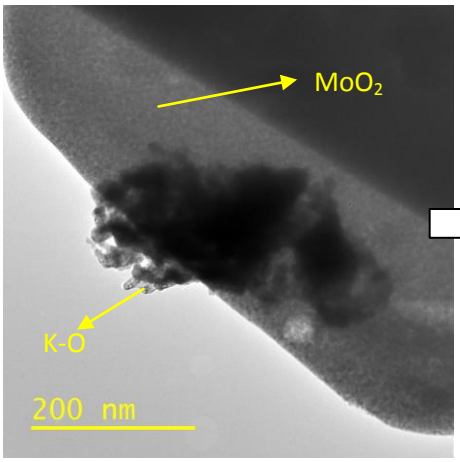

K-O located on MoO_2 in 1.3K-Mo_2N

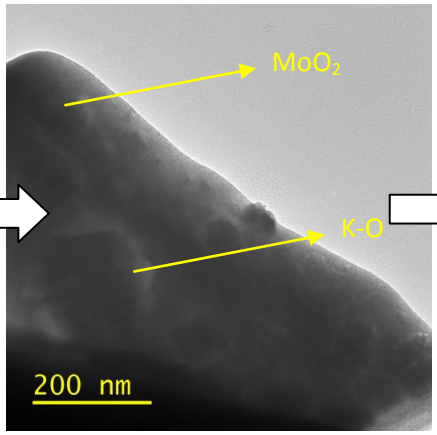

Chemical interaction between MoO_2 and K-O in 3K-Mo_2N

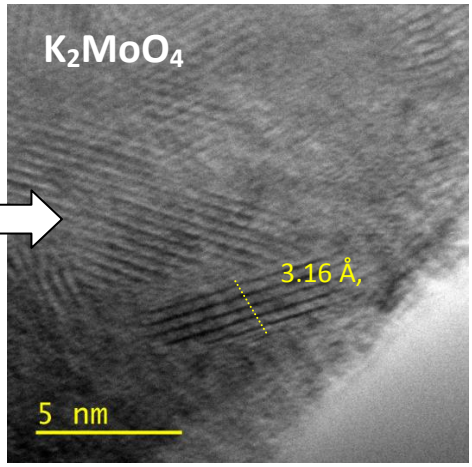

K_2MoO_4 formation in 6.2K-Mo_2N

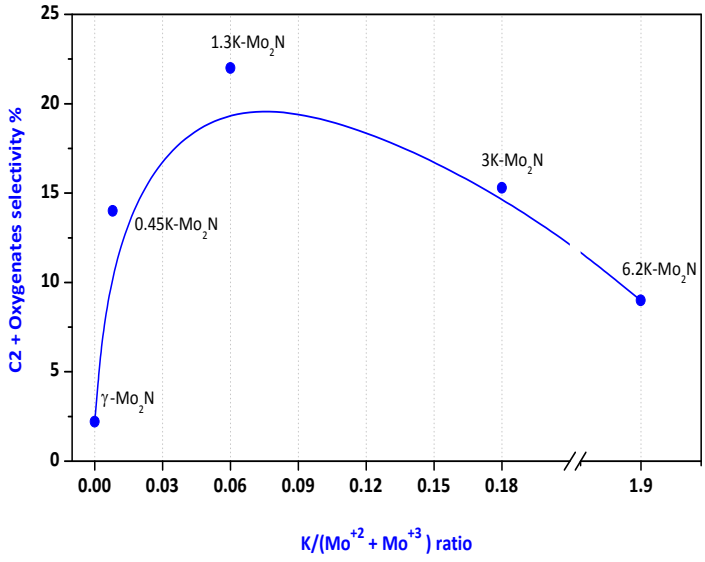

Highlights

CO hydrogenation to oxygenates was studied on Mo_2N for the first time.

CO conversion was decreased on K-Mo_2N compared to unpromoted Mo_2N.

Unpromoted Mo_2N showed higher hydrocarbon selectivity.

Improved C_2^+ oxygenates selectivity was observed on 1.3K-Mo_2N catalyst.

Well distributed K in the matrix of γ-Mo_2N improved the molecular CO adsorption.

Carbon monoxide hydrogenation on potassium promoted Mo_2N catalysts

Sharif F. Zaman[a, b, †], Nagaraju Pasupulety[b,*], Abdulrahim A. Al-Zahrani[a,b], Muhammad A. Daous[a,b], Saad S. Al-Shahrani[a], Hafedh Driss[a], Lachezar A. Petrov[b] and Kevin J. Smith[c]

[a] Chemical and Materials Engineering Department, Faculty of Engineering, King Abdulaziz University, P.O. Box 80204, Jeddah 21589, Saudi Arabia
[b] Center of Excellence in Catalysis, King Abdulaziz University, P.O. Box 80204, Jeddah 21589, Saudi Arabia
[c] Department of Chemical and Biological Engineering, University of British Columbia, Vancouver, BC, Canada

Abstract

The catalytic performance of Mo_2N and K-Mo_2N were assessed in hydrogenation of carbon monoxide in the reaction temperature range of 275-325 ^oC, 7MPa and 60,000 h^{-1}. The nitrides were synthesized via temperature-programmed treatment of ammonium heptamolybdate (AHM) and K-AHM precursors under continuous NH_3 flow. The influence of potassium loading (0.45 to 6.2 wt.%) on the Mo nitride phase and its resultant effect on the catalytic properties were been investigated. The nitride catalysts were characterized in terms of BET/pore size, powder X-ray diffraction, DRIFTs, CO-TPD-mass, HR-TEM and XPS measurements. The formation of cubic γ-Mo_2N and monoclinic K_2MoO_4 phases were confirmed by XRD and TEM. Platelet morphology with particle size in the range of 5-10 nm was observed for γ-Mo_2N. CO-TPD-mass results mainly revealed molecular CO sorption on Mo_2N and K-Mo_2N surface. The highest total oxygenate selectivity (44%, 300 ^oC) was observed on 1.3K-Mo_2N with a K/$Mo^{\delta+}$ surface ratio of 0.06. This is associated with well distributed K in the matrix of γ-Mo_2N. Distribution of K was reduced due to K_2MoO_4 formation at 3 and 6.2 wt.% K loading. DRIFTs results clearly demonstrates greater hydrocarbon formation on unpromoted Mo_2N due to (i) CO dissociative hydrogenation (ii) water-gas shift reaction. Further, addition of K to Mo_2N significantly improved the oxygenate selectivity by promoting the molecular CO insertion into –CHx intermediate.

Key words: Mo_2N catalysts, alkali metal, CO hydrogenation and higher oxygenates.

[†] Corresponding author. Tel.: +966 563063594; Fax : 966-2-6952257

E-mail address: zfsharif@gmail.com; sfzaman@kau.edu.sa

[*] Co-corresponding author. Tel.: +966 531596412

E-mail address: pasupulety@gmail.com; nsampathrao@kau.edu.sa

1. Introduction

Mixed alcohol synthesis from thermochemical conversion of syngas (synthesis gas: $CO+H_2$) is an important process for the production of oxygenate fuels and fuel additives. Majorly syngas is produced from the gasification of feedstocks such as coal, natural gas, biomass, shale oil and tar sands. Most important commercialized processes utilizing syngas are the production of synthetic gasoline via Fischer-Tropsch synthesis (FTs) reaction using iron (Fe) or cobalt (Co) based catalysts (eq. 1) [1-3], methanol synthesis using copper-zinc oxide (Cu-ZnO) based catalyst (eq. 2) [1,4]. Heterogeneous catalysts employed for the synthesis of ethanol and higher alcohols can be classified into four categories: (i) Modified methanol synthesis catalyst, (a) High temperature, Zn-Cr based catalyst (b) Low temperature, Cu-Zn based catalyst (ii) Modified FTs based catalyst (iii) Rhodium based catalyst (iv) Molybdenum based catalyst. Recently, Tan et al. [5] published isobutanol synthesis from syngas using alkali metal modified Cr/ZnO catalysts. Rh based catalysts show high selectivity to ethanol derived from syngas [6]. Cost and availability of Rh are the main barriers to the adaptation of this catalyst for commercial operation. Among other alternative higher alcohol synthesis catalysts, modified methanol synthesis catalysts selectively produce methanol and isobutanol, with low selectivity to ethanol [7]. Modified FTs based, Cu-Co catalysts show high yield to ethanol and higher alcohols, but they produce considerable amounts of hydrocarbons [8]. Among the molybdenum based catalysts K-MoS_2 shows very promising result for ethanol synthesis (40 C atom% selective to ethanol on CO_2 free basis) [9]. Recently Zaman and Smith [1, 10, 11] reported MoP based catalysts for higher alcohol synthesis, which also shows very interesting characteristics for C_2^+ oxygenate selectivity [43 C atom%]. β-molybdenum carbide catalyst also showed high activity for this reaction but suffers from high hydrocarbon selectivity [12].

1. FT type reaction

$CO+2H_2 \leftrightarrow -CH_2- + H_2O$ $\quad \Delta H_{298K} = -165$ kJ mol^{-1} eq. (1)

$CO + 3H_2 \leftrightarrow CH_4 + H_2O$ $\quad \Delta H_{298K} = -206$ kJ mol^{-1}

$CO + H_2O \leftrightarrow CO_2 + H_2$ $\quad \Delta H_{298K} = -41.1$ kJ mol^{-1}

2. CO insertion reaction

$CO + 2H_2 \leftrightarrow CH_3OH$ $\quad \Delta H_{298K} = -90.5$ kJ mol^{-1} eq. (2)

$CH_3OH + CO + 2H_2 \leftrightarrow C_2H_5OH + H_2O$ $\quad \Delta H_{298K} = -165.6$ kJ mol^{-1}

$C_2H_5OH + CO + 2H_2 \leftrightarrow C_2H_7OH + H_2O$ $\quad \Delta H_{298K} = -155.0$ kJ mol^{-1}

Recently, Hargreaves et al. [13, 14] reported the usage of metal nitrides for heterogeneous catalysis applications. The use of transition metal nitrides as hydrotreating catalysts are also reported [15-17]. The group VI transition metal nitrides exhibit comparable activity to that obtained with Pd and Pt based precious metal catalysts [16, 18] in hydrogen mediated reactions because of the contraction of the Mo d-band and modification of electron density due to the interstitial incorporation of nitrogen in the metal lattice [19]. A recent DFT study by Zaman [20] for CO adsorption and dissociation over γ-Mo_2N(111) plane reveals that CO dissociation has an activation barrier close to that of MoS_2(1001) plane, and concluded that it may show similar activity as of MoS_2 catalyst for syngas conversion.

In this study, we have established the feasibility of Mo_2N and K-Mo_2N as an active catalytic material for the CO hydrogenation to higher hydrocarbons and oxygenates. Until this moment, we were unable to find any study in the open literature dealing with the hydrogenation of CO to oxygenates and or to higher alcohols on potassium promoted molybdenum nitride. In this report, for the first time, we also present the drifts results on Mo_2N and 1.3K-Mo_2N catalysts for CO hydrogenation reactions.

2. Experimental

2.1. Catalyst preparation

Materials: Ammonium heptamolybdate ($(NH_4)_6Mo_7O_{24}\cdot 4H_2O$, Fluka ≥99.9%), anhydrous citricacid ($C_6H_8O_7$ ≥99%, Techno Pharmchem, Haryana, India) and potassium nitrate (KNO_3 ≥99%, Sigma-Aldrich) were obtained from their designated sources and used without any further purification.

For example, for the preparation of sample containing molybdenum nitride with 5 wt. % of nominal potassium loading requires 5.2 g of ammonium heptamolybdate, 5.7g of citric acid (CA) and 0.39g of KNO_3, which were dissolved in 100 cm^3 of deionized water under continuous stirring. The temperature of this solution maintained at 50 ^oC for 2 h for homogenization. Then the water was evaporated quickly by means of hot plate. The obtained pale yellow gel was cooked for 24 h using a water bath with temperature at 90 ^oC. The resultant foam like solid material was crushed to powder. Identical synthesis procedure was followed for unpromoted (no potassium containing sample), as well as for samples containing 1, 10 and 15 wt. % nominal potassium loading. For all the synthesized samples, molybdenum to citric acid mole ratio was

maintained at 1:1. All powdered samples were calcined at 500 ^{o}C for 4h under static air conditions. The calcined samples are named as Mo-CA, 1K-Mo-CA, 5K-Mo-CA, 10K-Mo-CA and 15K-Mo-CA. Here, the prefix 1, 5, 10 and 15 represents the nominal K loading wt.%.

All the calcined samples were subjected to stepwise temperature programmed ammonia treatment. One gram of the calcined sample was placed in a quartz reactor fitted with quartz frit. The nitridation procedure is as follows:

(i) In the first step, catalyst was kept at 120 ^{o}C for 30 min. under continuous He flow.

(ii) In the second step, gaseous ammonia was introduced to the catalyst bed with an approximate flow rate of 400 cm^3 min^{-1} and the reactor temperature was increased from 120 to 350 ^{o}C with a ramping rate of 1 $^{o}C.min^{-1}$.

(iii) In the third step, the catalyst temperature was increased from 350 to 700 ^{o}C with a ramping rate of 0.5 $^{o}C.min^{-1}$ and aged at this temperature for 2 h under continuous flow of ammonia.

(iv) In the fourth step, the reactor was cooled down to room temperature under He flow rate of 30 cm^3 min^{-1}.

(v) In the fifth step, the sample was passivated with flow of He containing 1 vol. % O_2 at a flow rate of 30 cm^3 min^{-1} for 1 h.

Finally, the catalyst was preserved in a glass bottle and unless otherwise stated, used for characterization studies and for catalytic activity tests.

Potassium content in passivated K-Mo_2N samples were analyzed by XRF and the results suggest that potassium loss took place during the nitridation process (Table 1). The passivated catalysts are denoted as Mo_2N, 0.45K-Mo_2N, 1.3K-Mo_2N, 3K-Mo_2N and 6.2K-Mo_2N. Here, the prefix 0.45, 1.3, 3 and 6.2 represents the actual weight percentage of potassium presented in Mo_2N.

2.2. Catalyst Characterization

The BET surface area and pore size analysis (using DFT method) of nitride samples were determined by Nova Station Quantachrome (USA) adsorption equipment at liquid nitrogen temperature after out gassing the samples at 200 ^{o}C under vacuum for 2 h. FTIR-ATR of the powdered samples were analyzed by using a Tensor-II spectrometer with ATR facility and OPUS software.

The X-ray diffractograms of the nitride samples were obtained on a EQUINOX 1000 Inel XRD instrument using Co K_α =1.7902Å with X-ray source generator settings at 40kV and 30mA with real time acquisition over 2θ of 110 degree. X-ray fluorescence (XRF) was performed using an Amptek XRF kits constituted of X-ray generator (mini-x) and X-ray detector (X-123SDD). The system was fitted with a silver source and operated at 50 kV and 30 mA. The data analyzed using the software XRF-TFR V1.33.

DRIFTs experiments were performed using a Bruker Tensor-II FTIR spectrometer equipped with a DLATGS detector at room temperature, Harrick praying mantis, high temperature and high pressure (with 4mm thick ZnS windows (≥ 6 MPa)) reaction chamber. Approximately, 0.1g of catalyst was loaded and reduced at 450 ^oC for 4h under the flow of H_2 (20 ml min^{-1}). Subsequently, the catalyst temperature was brought back to 300 ^oC under the flow of He and flush the reaction chamber for 1h. Then the reaction mixture (CO/H_2 1:1) gas was introduced into the chamber with an applied pressure of 5 MPa and collected the sample data.

Transmission electron microscopy (TEM), High resolution TEM images and energy dispersive x-ray analysis (EDS) of Mo_2N and K-Mo_2N samples were collected on a Technai 200 kV D1234 Super Twin microscope with camera length of 97 cm. Selected area electron diffractogram (SAED) analysis was performed using Diffraction ring profiler 1.7.

XPS results of Mo_2N and K containing Mo_2N samples was collected on SPECS GmbH high vacuum multi-technique surface analysis system equipped with Mg Kα 1253.6 eV X-ray source. The reported binding energy values are based on C 1s 284.8 eV.

Temperature programmed desorption (TPD) analysis of prepared samples was performed by adsorption-desorption of CO using Quantachrome Pulsar automated chemisorption instrument. The certified gas mixture of 14.95 vol. % CO in He and pure H_2 of 99.99% were supplied by Abdulla Hashim Gas (AHG), Saudi Arabia. In a typical experiment, approximately 0.1 g of nitride sample was pretreated under helium gas (10 cm^3 min^{-1}) at 200 ^oC for 1 h followed by hydrogen gas treatment at 450 ^oC for 4 h. Subsequently the catalyst was brought to room temperature and saturated with probe gas CO. Desorption of probe gas was performed in a temperature range of 30-400 ^oC at a ramping rate of 10 ^oC min^{-1} after 1 h of helium flushing. Mass analysis was performed using ThermoStarTM GSD 320 quad core mass spectrometer (Pfeiffer, Germany). The typical mass fragment inputs are as follows: m/z = 28 (CO) and m/z =

44 (CO_2). Desorption stream was analyzed simultaneously using a TCD and a mass detector by means of an automated split valve.

2.3. Catalytic activity tests

Catalytic activity tests were performed using a PID Eng and Tech system (Spain) equipped with a flow micro reactor, temperature, pressure and mass flow controllers. The mixture of CO: H_2 = 1:1 volume ratio was selected as model feed at 60,000 h^{-1} GHSV. Catalytic activity tests were carried out in the temperature range of 275 - 325 ^oC (±1 ^oC) with 25 ^oC step size at an applied pressure of 7 MPa (± 0.2 MPa). For example, 100 mg of nitride catalyst was loaded in to a copper lined stainless steel tube reactor (inside diameter 6.35mm and length 9.53mm) diluted with equal amount of quartz beads was treated with H_2 flow rate of 50 cm^3 min^{-1} at 450 ^oC for 4h. Subsequently, the H_2 flow was replaced by N_2 and reactor temperature was brought back to 275 ^oC. The reactant gas mixture CO: H_2 = 1:1 volume ratio was introduced with a flow rate of 100 cm^3 min^{-1} through an activated carbon trap (traps iron carbonyls formed inside the gas tank) into the reactor to attain the required pressure. After attaining the steady state (2h) at a set temperature and pressure of the reaction the reactor exit stream directed through a heated line at 160 ^oC to Agilent 7890A GC equipped with TCD, connected with Restek Plot Q column for CO and CO_2 separation, and to FID, fitted with HP Plot Q column for separation of hydrocarbons (methane, ethane, ethylene, propane, propylene and butane compounds) and oxygenates (methanol, ethanol, propanol, butanol, acetone, acetic acid, acetaldehyde and ethyl acetate) estimation. Same catalyst load was used for all the three temperatures. At each temperature five data points were collected. The empty copper lined reactor showed negligible CO conversion (≤0.1%) under identical reaction conditions. The reported results are within the error range of ± 0.1%. The syngas conversion and selectivity of the products [10] were calculated according to the following equations:

$$\text{CO conversion (mass \%)} = \frac{\text{CO initial moles} - \text{CO final moles}}{\text{CO initial moles}} \text{ X } 100 \qquad (3)$$

$$\text{Selectivity (mass \%)} = \frac{n_i C_i \text{ product}}{\sum n_i C_i} \text{ X } 100 \qquad (4)$$

where, n_i is the number of carbon atoms contained in the molecule of the i^{th} component and C_i is the mole fraction of i^{th} component in the reaction mixture at the reactor exit.

3. Results and discussion

3.1. X-ray powder diffraction analysis

Powder X-ray diffraction patterns of calcined (550 ^oC, 4 h under static air) samples are presented in Fig. 1a. The calcined samples principally shows X-ray diffraction patterns at 2θ equal to 15.0, 27.4, 30.0, 32.0, 34.6, 38.8, 39.6, 45.6, 46.5, 53.6, 54.2, 57.9, 58.8, 62.3, 63.9, 65.0, 66.7, 68.0 and 69.5°. These peaks are consistent with the presence of orthorhombic MoO_3 phase [PDF 00-005-0508]. Identical X-ray signals are pronounced due to the presence orthorhombic MoO_3 up to 5K-Mo-CA predominantly. Polycrystalline phases such as, $K_3Mo_{14}O_{22}$ [PDF 01-086-243] and $K_6Mo_{10}O_{33}$ [21] are observed in 10K-Mo-CA and 15K-Mo-CA samples (Fig. 1a, green and magenta lines) which are resulted due to the chemical interaction between K and Mo-O. The MoO_3 phase in 15K-Mo-CA is reduced significantly compared to other calcined samples. Further, the unindexed X-ray reflections at 2θ equal to 39.0, 39.5, 40.0, 44.0 and 50.0° in 10K-Mo-CA and 15K-Mo-CA samples are probably due to the presence of other polycrystalline K-Mo-O phases.

Powder X-ray diffraction patterns of passivated Mo_2N and K-Mo_2N samples are presented in Fig.1b. The -NH_x species which are formed during the ammonolysis process above 500 ^oC, are adsorbed on the coordinatively unsaturated sites existing on the surface of Mo_2N [22]. A rapid autothermal oxidation of adsorbed -NH_x species take place upon exposure to air. To prevent the spontaneous reaction a careful passivation by oxygen provides a protective layer on Mo_2N surface by eliminating most of the bonded -NH_x species [22]. The diffraction pattern of (Fig. 1b, black line) unpromoted Mo_2N showed X-ray reflections at 2θ equal to 43.7, 50.8, 75.0, 90.8 and 96.0° that can be associated, respectively, with (111), (200), (220), (311) and (222) planes of cubic γ-Mo_2N crystallographic phase [PDF 00-025-1366]. Identical X-ray patterns are observed up to 1.3K-Mo_2N due to the presence of cubic γ- Mo_2N phase. Along with the cubic γ-Mo_2N phase, unpromoted Mo_2N sample showed X-ray patterns at 2θ equal to 30.0, 62.5, 71.5 and 79.0° with respective planes (-111), (211), (310) and (-402), which are consistent with monoclinic MoO_2 phase [PDF 00-078-1070]. The formation of the partially reduced molybdenum oxide, such as MoO_2 during the reduction-nitridation process was also reported in reference [23, 24]. Nagai et al. [25] also recorded the formation of MoO_2, γ-Mo_2N, β-Mo_2N and

metallic Mo during the treatment of MoO_3 with NH_3 at temperatures up to 900 ^oC. No crystallite phases related to potassium oxide is detected in the prepared nitrides for K concentration below 1.3 wt.% (1.3K-Mo_2N). This observation might be associated with the presence of highly dispersed potassium crystallites, sized less than 4nm, which are below the detection limit of X-ray diffraction method. The 3K-Mo_2N sample shows the presence of cubic γ-Mo_2N, hexagonal δ-MoN and monoclinic K_2MoO_4 phases. At 6.2 wt. % of potassium content the sample primarily displays δ-MoN, K_2MoO_4 phases along with minor portion of cubic γ-Mo_2N. It is, however, worth noting that with the increase of K loading in Mo_2N, the amount of the MoO_2 phase was decreased due to the chemical interaction between K and Mo-O, resulted in formation of the K-Mo-O crystals. The observed crystallographic changes from the calcined to nitridation-passivation samples can be summarized as follows:

(i) Orthorhombic MoO_3 precursor upon nitridation-passivation primarily yields cubic γ- Mo_2N phase.

(ii) Hexagonal δ-MoN is an intermediate phase to produce cubic γ- Mo_2N from MoO_3 and or from MoO_2 nitridation-passivation [13]. In the present work, molybdenum chemically interacts with K at 6.2 wt.% and eventually yields K_2MoO_4. Due to this, hexagonal δ-MoN to cubic γ-Mo_2N phase transformation was limited at this loading.

(iii) Prominent K_2MoO_4 phase appeared due to decomposition of the polycrystalline K-Mo-O precursors and/or potassium oxide interaction with MoO_2.

(iv) Molybdenum nitride structure was intact even after K addition.

3.2. BET surface area and pore size analysis

All registered isotherms, shown in Fig.2a, are type *IV* with *H4* hysteresis loop. The type *H4* loop is often associated with narrow slit-like pores [26]. Fig.2b shows the tri-modal pore size distribution for Mo_2N. The micropores have an average pore diameter below 20 Å while the mesopores have an average pore diameter between 22 and 55 Å. The mesopores of Mo_2N themselves have bimodal distribution in the range of 22-35 Å and 35-55 Å. Upon the incorporation of K into Mo_2N the number of micropores was significantly reduced and new mesopores were formed with an average pore diameter in the range of 22-40 Å. It is noteworthy that, no micropores were found in 6.2K-Mo_2N sample. The pore volume and BET surface area

data for prepared samples are presented in Table 1. The BET surface area decreased significantly from 110 $m^2 g^{-1}$ to 10 $m^2 g^{-1}$ after the incorporation of 0.45wt. % of K into Mo_2N.

Citric acid was used as a chelating component for promoting the BET surface area of tungsten phosphide (WP) [27] and molybdenum phosphide (MoP) [28] catalysts. It is playing a role of chelating/bridging agent between the metal ions. In this study, the obtained high surface area of 110 $m^2 g^{-1}$ for Mo_2N, in the presence of cheating agent citric acid, was associated with the formation of molybdenum citrate [29]. However, the BET surface area decreased with K addition to citric acid induced synthesis of Mo_2N catalysts. Lower BET surface area was reported for potassium promoted MoS_2 with mesopore texture compared to the parent MoS_2 having micro and mesopore texture. The authors suggested that the decrease in the BET surface area for K-Mo_2S was probably a result of the intercalated K-water species in between the MoS_2 slabs [30]. Lower BET surface area was also reported for 10 wt.% K supported on Mo_2C and it was attributed to Mo_2C pore blockage by K_2CO_3 [31].

In this work, the significant decrease in the BET surface area for K promoted samples might be associated with melting of K and or K/Mo salts to some extent during ammonolysis at elevated temperatures, which might led to pore blockage. Further, MoO_3-potassium oxide binary phase diagram shows, at around 450-600 ^oC, the existence of liquid K-phase composed of different potassium oxides KO_2, K_2O_2 and K_2O [32].

3.3. XPS analysis

K 2p, Mo 3d and N KLL (Auger) orbital XPS analysis of K-Mo_2N passivated samples are presented in Fig. 3A, 3B and 3C respectively. The corresponding surface composition data are summarized in Table 2. K 2p region is composed of a doublet with contributions at 292.5 and 295.5 eV which are, respectively, assigned to K $2p_{3/2}$ and K $2p_{1/2}$ lines [33]. These XPS signals are exhibited due to the presence of K_2O or K_2MoO_4 species on the surface of K-Mo_2N samples. However, at 6.2wt. % K loading, the sample shows an additional shoulder at 291 eV, which might be associated with the presence of impurity of carbonates coming from the potassium nitrate precursor. Similar XPS results were reported by Galvez et al. [34] for Fe-K/Al_2O_3 samples.

The deconvoluted Mo 3d XPS result (Fig. 3B) shows several oxidation states ranging from Mo^{6+} to Mo^{2+}. After deconvolution of unpromoted Mo_2N, Mo $3d_{5/2}$ and $3d_{3/2}$ transition pairs appeared at binding energies of 228.4 and 231.6, 229.2 and 232.3, 230.2 and 233.7, 232.5 and

235.4 eV. The Mo 3d $_{5/2}$ signal attributed to Mo^{2+} at 228.6 eV, Mo^{3+} at 229.2 eV, Mo^{4+} at 230.2 eV and Mo^{6+} at (232.5 eV) species [29]. Identical signals of Mo $3d_{5/2}$ were pronounced for samples containing up to 1.3 wt.% K due to the presence of similar Mo species. The above signals marginally shifted to lower binding energies by 0.4 eV for 3K-Mo_2N sample. Which suggests Mo 2+ and 3+ reduction towards Mo^0 started at this loading. For 6.2K-Mo_2N, Mo 3d XPS pattern was completely changed compared to unpromoted Mo_2N and other K-Mo_2N samples. Interestingly, Mo^{4+} and Mo^{6+} species were dominating over Mo^{2+} species and a new shoulder appeared at 227.0 eV might be associated with the presence of metallic Mo species [35] for 6.2K-Mo_2N sample. It is noteworthy that, no Mo^{3+} species were detected at this K loading. Hence, at higher K loading metallic Mo formation suggests the reduction of Mo^{3+} and or Mo^{2+} species. This might be associated with ease of reduction of low valence Mo species (δ-MoN) under nitridation conditions. Among the studied K-Mo_2N samples, Mo 3d distributions (Table 2) varied significantly. In the present study, the Mo^{4+} valence species are related to MoO_2 and or K_2MoO_3 phase and Mo^{6+} valence species might be associated with MoO_3 and or K_2MoO_4 phase in agreement with XRD data.

XPS induced Auger spectra of the passivated K-Mo_2N samples are presented in Fig.3C. The major Auger signal appeared at 383 eV with a shoulder at 389 eV. However, these signals shifted to higher kinetic energy and the major signal appeared at 386 eV with a shoulder at 391 eV for 6.2K-Mo_2N. Kawai et al. [36] reported Auger transitions at 385 and 392 eV for molybdenum nitride samples. The transition at 385 was attributed to $KL_{2,3}L_{2,3}$ level of the nitrogen atom in the nitride and the later transition at 392 eV was due to L level of nitrogen to $N_{4,5}$ level of molybdenum. Hence, the higher kinetic energy transitions are likely due to the nitrogen chemical environment of hexagonal δ-MoN and the lower energy transitions related to nitrogen chemical environment of cubic γ-Mo_2N phase.

The surface Mo species distribution and surface ratio of K:(Mo^{2+}+ Mo^{3+}) and N: (Mo^{2+}+ Mo^{3+}) are summarized in Table 2. Among the K promoted catalysts the surface Mo^{2+} + Mo^{3+} species (denoted as $Mo^{\delta+}$ in the literature related to γ-Mo_2N) had the highest concentration at 1.3 wt. % K loading. On the other hand Mo^{4+} and Mo^{6+} species were decreased in samples containing up to 1.3 wt. % K loading and increased in samples with higher K loadings. The results indicate that the K-O mainly dispersed on Mo^{4+} and Mo^{6+} species up to 1.3K-Mo_2N

sample (Fig. 4a, TEM image). Whereas, the surface abundance of Mo^{4+} and Mo^{6+} species for 3K- and 6.2K-Mo_2N suggests K-Mo-O (K_2MoO_3, K_2MoO_4) phases.

3.4. TEM/HRTEM/SAED measurements

The passivated K-Mo_2N samples were examined by TEM/HRTEM/SAED techniques and the representative images are shown in Fig. 4. The TEM image of 1.3K-Mo_2N catalyst (Fig. 4a) showed bar like morphology for MoO_2, which might be characterized by Mo-O-Mo links. The potassium species were found with spherical shape located on the MoO_2 bar like structures of 1.3K-Mo_2N. The high-resolution image of the corresponding slot on 1.3K-Mo_2N (Fig. 4b) showed an average d-spacing of 3.71 Å, consistent with the (111) plane of dipotassium oxide (K_2O) with an average particle size of 2-3 nm. Further, the SAED (inset, Fig.4b) analysis yielded d- spacing of 2.26, 1.85 and 1.44 Å, consistent respectively, with the (202), (222) and (402) planes of K_2O [ICSD 96-101-0879]. The chemical interaction between K_2O and MoO_2 has been clearly established in Fig. 4c for the sample containing 3wt. % of potassium in Mo_2N. Fig. 4d for 6.2K-Mo_2N catalyst revealed the d spacing of 3.16 Å, consistent with (310) plane of K_2MoO_4 [PDF 029-1021]. Plate like morphology was observed for γ-Mo_2N in potassium promoted samples (example image of 3K-Mo_2N presented as Fig. 4e). Further, homogeneous distribution of these platelets with particle size range of 5-10 nm (Table 1) illustrated in supplementary image S1a. The inset of Fig. 4e shows SAED of γ-Mo_2N phase. Within B1-structured nitrides, one fcc lattice is defined by the transition metal atoms, and the N atoms are presumed to occupy interstitial octahedral sites to form the second interpenetrating fcc lattice. Vacancies on the anion sublattice result in non-stoichiometric nitrides such as Mo_2N. Hence, the observed platelet type particles might be associated with octahedral N atoms within the fcc lattice of Mo atoms [37]. The careful analysis of 6.2K-Mo_2N by HRTEM/SAED (Fig. 4f) yields significant information about the structure of hexagonal δ-MoN phase where these particles are also of plate type and located on the large plates of γ-Mo_2N (S1c). The SAED reveals average d-spacing of 2.48 Å consistent with (200) plane of δ-MoN. Similar SAED results was observed by Ganin et al. [38] for MoN thin films and attributed to distorted NiAs type structure with triangular clusters of Mo atoms and a centered N atom.

In conclusion, TEM/HRTEM/SAED results revealed the chemical interaction between K and Mo-O and have form the K-Mo-O species (K_2MoO_3 and or K_2MoO_4) in agreement with

XRD/XPS data. Hexagonal δ-MoN plates characterized by thin in nature exists on the big plates of γ-Mo_2N. The distributed K content in to the Mo_2N matrix estimated by parallel beam EDS showed in Table 1. The greater K content observed at 1.3wt.% K loading suggests greater K distribution in the Mo_2N matrix which played a vital role in oxygenates formation during CO hydrogenation.

3.5. CO-TPD-mass measurements

Fig. 4 shows the CO-TPD-mass results on reduced Mo_2N and K-Mo_2N samples. Two distinct desorption peaks were observed for Mo_2N with peak maxima at 150 and 300 ^oC for m/z=28 (Fig.4a). The earlier CO desorption peak was assigned to the linearly adsorbed CO on the surface molybdenum atom of 2+ and 3+ valence state (Mo-C≡O). The later CO desorption peak assigned to NCO species, resulted from CO adsorbed on the surface N sites [39]. Similar, mass signals were pronounced due to Mo-CO and N-CO species up to 1.3 wt.% potassium loading. However, Mo-CO sorption was considerably reduced for 3K- and 6.2K- loadings compared to 1.3K-Mo_2N. The results are in agreement with XPS data where surface $Mo^{\delta+}$ species was found to be low for 3K- and 6.2K-Mo_2N. In addition, at 6.2K- loading an extended CO desorption signal was observed in the temperature range of 225-400 ^oC with signal maxima at 320 ^oC. This is associated with metallic Mo sites, where CO dissociates to produce carbon and recombination of adsorbed C and O desorb as CO below 340 ^oC on Mo_2N surface [40]. Fig. 4b presents m/z=44 (CO_2) sorption results for Mo_2N and K-Mo_2N samples. A negligible amount of CO_2 was observed over the Mo_2N and up to 3 wt.% K-Mo_2N. However, considerable amount of CO_2 desorbed at 325 ^oC on 6.2K-Mo_2N. This is likely due to the presence of metallic Mo sites (as evidenced by XPS analysis) which dissociates CO and produce CO_2 [41]. Thompson et al. [40] found that CO partially dissociated on bulk Mo_2N. Yang et al. [39] reported that majority of CO is adsorbed molecularly on Mo_2N/Al_2O_3 surface. Our CO-TPD-mass results principally showed the molecular CO sorption, which was also reported by Zaman [20] through DFT study over γ -Mo_2N (111) plane.

Influence of K addition to Mo_2N on the CO sorption is as follows:

(i) Principally molecular CO sorption was observed on Mo_2N and K-Mo_2N catalysts.

(ii) CO_2 formation indicates CO dissociation on these catalysts.

(iii) Well distributed K in Mo_2S slabs improved the back donation of Mo and stabilizes $Mo^{\delta+}$ sites [42]. In the present work, the good distribution of K observed in 1.3K-Mo_2N and exhibited greater molecular CO sorption.

(iv) K_2MoO_4 formation reduces the K distribution in to Mo_2N, hence, lowers molecular CO sorption for 3K- and 6.2K-Mo_2N.

3.6. FTIR-DRIFTs analysis

The insitu FTIR-DRIFTs analysis on Mo_2N and 1.3K-Mo_2N catalysts was performed at 300 ^oC, 5 MPa with CO:H_2 feed 1:1 volume ratio and the results are presented as Fig. 6a &b. The unprompted Mo_2N showed the formation of hydrocarbons, mainly methane and CO_2 from the beginning of the reaction at 3015 and 2355 cm^{-1} respectively. The hydrocarbons and CO_2 formation was increased with the increase in reaction time indicates greater hydrogenation tendency of unprompted Mo_2N. The CO_2 formation mainly associated with water-gas shift reaction. CO dissociative hydrogenation reported on the surface of Mo_2N to produce methane as first hydrocarbon and water as a byproduct [40]. The improved relative intensity of methane (3015 cm^{-1}) in Fig. 6a, time resolved spectra suggest CO dissociative hydrogenation under reported reaction conditions. Further, the relative intensity of CO_2 was also increased and the separation between CO and CO_2 was decreased with time. The result indicates that CO_2 concentration is almost equal to CO at reactor zone after 3h of reaction. On the other hand, hydrocarbons in the stretching frequency range of 2850-3000 cm^{-1} and 3050-3200 cm^{-1} also increased with reaction time, which reveals the chain propagation under the hydrogen rich environment was created due to water-gas shift reaction. After 30 min. of reaction, a new contribution appeared in the frequency range of 950-1080 cm^{-1} centered at 1025 cm^{-1} is attributed to the formation of alcohols (methanol and ethanol). After 1h of reaction, bands appeared between 1480 and 1680 cm^{-1} suggests the formation of other oxygenates such as esters.

Time resolved DRIFTs analysis on 1.3K-Mo_2N catalyst at 300 ^oC, 5MPa is presented as Fig.6b. Potassium promoted catalyst significantly reduced the formation of hydrocarbons particularly methane and CO_2 at the initial stages of reaction (up to 45 min.) compared to unpromoted Mo_2N. However, after 1h of reaction the relative formation of hydrocarbons and CO_2 were increased. The results indicate CO dissociative hydrogenation and water-gas shift reactions occurred at slower pace on this catalyst. The alcohol formation at 1025cm^{-1} increased from 1h to 3h of reaction time with consistent hydrocarbon formation. It suggests molecular CO

insertion to –CHx intermediate to form –CxHyO (acyl) intermediate to produce alcohols on this catalyst surface. Hence the CO activation is different on K distributed Mo_2N compared to unpromoted Mo_2N. Similar results were reported by Santos et al. [42] on K-MoS_2 catalyst for alcohol synthesis from syngas. The authors suggested that K occupies the edges and corners of MoS_2 by removal of sulfur and creates coordinative unsaturated sites ($Mo^{\delta+}$) with different chemical environment, which decreases the hydrogenation ability of K-MoS_2. Stabilized alkoxy or methoxy (–CHxO) species on the K-Mo_2N surface desorb in the form of methanol. The presence of K, in close vicinity to an adsorbed methyl group, will favor CO insertion, stabilizing acyl intermediates that are further hydrogenated to ethoxy and finally to ethanol or higher alcohols.

3.7. Catalytic activity results

The CO_2 selectivity was obtained in the range of 50-60% in the temperature range of 275-325 ^oC on unpromoted Mo_2N. On the other hand, observed CO_2 selectivity was 40-50% on K-Mo_2N catalysts. High selectivity to CO_2, due to the water gas shift reaction, was reported on Mo based catalysts such as Mo_2C and Mo_2N [40].

Fig. 7a shows the influence of K loading on CO hydrogenation product distribution in the temperature range of 275-325 ^oC, 7 MPa and 60,000 h^{-1}. The CO conversion increased with increase in the reaction temperature and reached to a maximum value of 10% on γ-Mo_2N at 325 ^oC. The K promotion up to 1.3wt.% decreases the conversion to 4.5% and slightly improves the conversion to 7 % after this loading at 325 ^oC. The decrease in the conversion at 1.3 wt. % of K loading might be associated with partial blockage of Mo sites by K_2O (TEM Fig. 4a), which contributes to the CO hydrogenation to some extent. After this loading (3 and 6.2 wt.%), the surface present metallic Mo sites slightly improved the CO conversion and mostly contributed to hydrocarbons. In addition, at 3 and 6.2 wt.% K loading, N-CO sorption (CO-TPD results) was slightly improved compared to 1.3K-Mo_2N. The results indicate that surface N sites (Table 2) can also influence the CO conversion. Further, selectivity to hydrocarbons was increased with the increase in reaction temperature (Fig. 7a). Andersson et al. [30] also noted increased hydrocarbon selectivity with the increase in the reaction temperature on K-Ni-MoS_2 catalysts. The authors hypothesized that alcohols can undergo hydrogenation/dehydration to form hydrocarbons at higher reaction temperatures. Higher temperatures (upon reaching the

equilibrium) are also favorable for the formation CO_2 via water gas shift reaction, consistent with the results reported for K/Mo_2C catalysts [31]. In addition, increased CO_2 concentration at higher temperatures can also alter the CO/H_2 ratio in the reactor zone and further influence the CO insertion process followed by higher alcohol formation [43-45]. Our DRIFTs data clearly demonstrates enhanced CO_2 formation via water gas shift reaction on unpromoted Mo_2N. Hydrocarbon formation, particularly methane formation in CO hydrogenation on Mo based catalysts are reported as Mo metal (Mo^0) > Mo_2N ($Mo^{\delta+}$) > MoO_2 (Mo^{4+}) > MoO_3 (Mo^{6+}) [46]. Therefore, in the present work the hydrocarbon formation is mainly associated with $Mo^{\delta+}$ and Mo^0 sites. Further, K addition to γ-Mo_2N at 1.3wt.% loading significantly reduces the hydrocarbon formation due to improved molecular CO insertion in to hydrocarbon intermediate via K-$Mo^{\delta+}$ sites (Scheme 1). Tavasoli et al. [47] reported reduced hydrocarbon formation during CO hydrogenation on K_2MoO_4 phase. Based on these reports Mo in +6 valence state was found to be less active for hydrocarbon formation. In FTs, α value indicates the formation of long-chained hydrocarbons. Methane will always be the largest single product as long as α is less than 0.5, however, by increasing α close to one, increases the formation of long-chained hydrocarbons [48]. In the present study, α value obtained as 0.40 for unpromoted Mo_2N. On the other hand, 0.39, 0.38, 0.40 and 0.42 (α value) was observed for 0.45K-, 1.3K-, 3K- and 6.2K-Mo_2N samples respectively, at 300 ^oC. The results suggest that at higher K loadings greater C_2^+ hydrocarbons formation over lower K loadings.

Among the studied catalysts 1.3K-Mo_2N showed maximum total oxygenates selectivity of 50, 44 and 34% at 275, 300 and 325 ^oC respectively. DRIFTs results showed molecular CO insertion into hydrocarbon (–CHx) intermediate and further hydrogenation of resultant intermediate yielded oxygenates at this loading. This was likely due to well distribution of K into Mo_2N matrix, stabilizes $Mo^{\delta+}$ state by back donation of electrons. At higher loadings (3 and 6.2 wt.%) most of the K chemically interacted with molybdenum oxide and produced K_2MoO_4. The distribution of K into the Mo_2N matrix was effected by this phenomenon. On the other hand, K loading was inadequate at 0.45 wt.% to produce oxygenates. The results in terms of oxygenate selectivity indicates the optimum potassium loading was at 1.3 wt.%.

3.8. Alcohol distribution

The distribution of alcohols on γ-Mo_2N and K-Mo_2N catalysts are illustrated in Fig. 7b. The butanol selectivity was found to be <1 % at all K loadings and was included in other liquid

products selectivity. Unpromoted Mo_2N showed only 4% of methanol selectivity followed by ethanol (1 %) and other liquid products (butanol, acetone and ethyl acetate) selectivity (1 %) at 300 ^oC. On the other hand, methanol selectivity was increased considerably to 22 % at 1.3wt. % of K promotion in γ-Mo_2N. At the same time ethanol, propanol and other liquid product selectivity improved to 6, 7 and 9 % respectively. At higher K loadings (3 and 6.2 wt. %) methanol, ethanol, propanol and other liquid product selectivity was decreased at 300 ^oC. This is associated with reduced capacity for molecular CO adsorption followed by molecular CO insertion. Increase in the reaction temperature to 325 ^oC decreases the alcohol selectivity for all the studied catalysts. This is associated with improved hydrogenation tendency of these catalysts via water gas shift reaction [31, 43-45]. One of the conventional aspects, for the formation of higher alcohols from syngas is that the catalyst should be able to adsorb CO molecularly as well as dissociatively. Molecular CO adsorption leads to methanol formation as a first alcohol product, while dissociate CO adsorption give rise the $–C_xH_y$ intermediate and eventually to hydrocarbons. The existence of both sites on the catalyst surface leads to higher alcohol formation via insertion of molecular CO in to the $–C_xH_y$ intermediate [48, 49]. Christensen et al. [50] recently reported the possibility of alcohol coupling, which intern led to condensation type of reactions for the formation of n-propanol and n-butanol on alkali promoted MoS_2 catalysts.

In the present study, among the alcohol distributions, methanol was the major product and the results are in line with results of the CO-TPD-mass studies where the CO principally adsorbed molecularly. Jiang et al. [51] reported K-Mo-S species formation at lower K loadings and K aggregation at higher loadings, which lead to blockage of the co-ordinatively unsaturated sites favoring hydrocarbon formation. We found K distribution in the γ-Mo_2N matrix by TEM/EDS analysis (Table 1, supplementary figure S1a & b). The ATR-FTIR results of K-Mo_2N samples (supplementary figure S3) shows FTIR band for Mo-N vibration at 665 cm^{-1}. Further, Mo-O stretching vibrations in the finger print region of 700-975 and 600-650 cm^{-1} was observed for K-Mo_2N samples. These vibrations are attributed to polycrystallites of -MoO_4 and -Mo_4O_{13} phases of K. However, a new shoulder appeared at 680 cm^{-1} for K-Mo_2N samples was likely due to K-Mo-N species. The decreasing order of total alcohol formation at 300 ^oC is as follows: 1.3K-Mo_2N (35%) > 3K-Mo_2N (27%) > 0.45K-Mo_2N (23%) > 6.2K-Mo_2N (21%) > Mo_2N (5%). The overall result (EDS, FTIR and activity) suggests that, K distribution was good at 1.3 wt.% of K loading in to Mo_2N. Aggregation of K as K_2MoO_4 or $K_2Mo_4O_{13}$ started at 3 wt.% and

intensified at 6.2 wt% K loading. Further, the distributed K helps to stabilize the $Mo^{\delta+}$ species by back donation of electrons and improves the molecular CO insertion (K- $Mo^{\delta+}$).

Further, olefins (mainly ethylene and propylene) selectivity was increased from Mo_2N (5 %) to 1.3K-Mo_2N (8%) and decreased slightly on 3K- (7%) and 6.2K-Mo_2N (6.5%). This is associated with transformation of corresponding alcohol and or alcohol intermediate dehydration to olefins under the reaction conditions.

3.8.1. Influence of space velocity

The product distribution as a function of GHSV on 1.3K-Mo_2N at 300 ^oC, 7MPa is presented in Fig. 8a. At higher space velocity (60,000 h^{-1}) approximately, 4.5 % of CO was converted into hydrocarbons and oxygenates with selectivity of 50 and 44 %, respectively. At lower space velocity (15000 h^{-1}), CO conversion was increased to 28 % with 76 % of hydrocarbon and 16% of total oxygenate selectivity. Further, the C_2^+ hydrocarbons selectivity was increased with decrease in the space velocity of the reaction mixture. In addition, methanol selectivity was reduced (difference between total oxygenates and C_2^+ oxygenate selectivity in Fig. 8a) at lower space velocity. The results indicate that hydrocarbon chain propagation followed by CO insertion is favorable to form C_2^+ oxygenates at lower space velocity. It is noteworthy that, unknown product selectivity (100-(total hydrocarbons + total oxygenates)) is also increased with decrease in the space velocity.

3.8.2. Correlation between K/$Mo^{\delta+}$ surface ratio and C_2^+ oxygenates

The selectivity to C_2^+ oxygenates at 300 ^oC is plotted as a function of K: $Mo^{\delta+}$ surface ratio of K-Mo_2N catalysts in Fig.8b. Unpromoted cubic γ-Mo_2N showed only 2.2 % of C_2^+ oxygenate selectivity. Whereas, the C_2^+ oxygenate selectivity was improved to 14 % by addition of small amount of K (0.45 wt. %). Further, C_2^+ oxygenate selectivity reached to a maximum value of 22 % at 1.3wt.% of K loading in Mo_2N. At 3 & 6.2 wt.% K loadings the C_2^+ oxygenate selectivity was decreased to 15 and 9 % respectively. In this study, the highest C_2^+ oxygenate selectivity on 1.3K-Mo_2N is associated with Molecular CO adsorption followed by efficient insertion into –CHx.

3.9. Time on stream study

The time on stream results on unpromoted Mo_2N and 1.3K-Mo_2N are presented in Fig.9. It is obvious from the results that the catalytic activities are quite consistent for 10h of CO hydrogenation at 300 ^oC, 7Mpa and 60,000 h^{-1}. Unpromoted Mo_2N showed around 92% of hydrocarbons and 5% of alcohols selectivity at 5% of CO conversion. On the other hand, K promoted Mo_2N exhibited around 50% of hydrocarbons and 35% of alcohols selectivity at 2.5% of CO conversion. The results suggest that the deactivation of molybdenum nitride catalyst is slow under the studied reaction conditions.

Fig.10 shows the XRD patterns for 1.3K-Mo_2N at different stages of its treatment such as nitridation-passivation at room temperature for 1h under 30 cm^3 min^{-1} gas flow rate of 1% O_2-He, reduced at 450 ^oC, for 4h under 50 cm^3 min^{-1} gas flow rate of 99.99% H_2 and spent in the CO hydrogenation reaction at 325 ^oC, 7MPa and 60,000 h^{-1} GHSV. It is obvious from the results that passivated and spent catalysts principally showed cubic γ-Mo_2N with small portion of MoO_2 phase. However, MoO_2 formation slightly improved for the spent catalyst indicates that partial oxidation of $Mo^{\delta+}$ species during the reaction. Further, reduced catalyst principally showed MoO_2 phase with minor cubic γ-Mo_2N phase. The MoO_2 phase formed due to the exposure of catalyst to air during the XRD analysis. The results indicate that after reduction at 450 ^oC, catalyst surface was enriched in $Mo^{\delta+}$ species and oxidized to MoO_2 up on exposure to air. In conclusion, fresh to reduce to spent Mo_2N (S2) and 1.3K-Mo_2N (Fig.10) catalysts XRD results clearly demonstrate the intact molybdenum nitride structure after the addition of K as well as after 10 h of reaction.

4. Conclusions

Unpromoted Mo_2N showed higher hydrocarbon selectivity than K promoted Mo_2N catalysts. This is associated with CO dissociative hydrogenation followed by water gas shift reaction on $Mo^{+\delta}$ sites. The structure of molybdenum nitride was intact even after the incorporation of K in to it. K promotion to Mo_2N led to (i) improved molecular CO sorption (ii) improved molecular CO insertion into –CHx intermediate. Among the K-Mo_2N catalysts 1.3K-Mo_2N showed greater selectivity to total oxygenates during CO hydrogenation. This is associated with well distribution of K into Mo_2N matrix led to K-$Mo^{+\delta}$ species, which improves the molecular CO insertion. At higher potassium loadings (3 and 6.2 wt.%), K_2MoO_4 formation has reduced the K distribution in to Mo_2N matrix, which effects the molecular CO insertion.

5. Acknowledgements

The project funded by the National Plan for Science, Technology and Innovation (MAARIFAH)-King Abdulaziz City for Science and Technology - the Kingdom of Saudi Arabia, award number (12-PET2720-03). The authors also, acknowledge with thanks Science and Technology Unit, King Abdulaziz University for technical support.

6. References

[1] S. Zaman, K.J. Smith, Cat. Rev. -Sci. Eng. 54 (1) (2012) 41–132.
[2] D. Leckel, Ind. Eng. Chem. Res. 23 (2009) 2342–2358.
[3] A.Y. Khodakov, W. Chu, P. Fongarland, Chem. Rev. 107 (2007) 1692–1744.
[4] W. S. Cheng, H.H. Kung, (Eds.), Methanol Production and Use; Marcel Dekker Inc.: New York, 1994.
[5] L. Tan, G. Yang, Y. Yoneyama, Y. Kou, Y. Tan, T. Vitidsant, N. Tsubaki, Appl Catal. A: Gen. 505 (2015) 141–149.
[6] V. Abdelsayed, D. Shekhawat, J. A. Poston Jr., J. J. Spivey, Catal. Today 207 (2013) 65–73.
[7] R.G. Herman, Cat. Today 55 (2000) 233–245.
[8] P. Chaumette, Ph. Courty, A. Kiennemann, R. Kieffer, S. Boujana, G. A. Martin, J. A. Dalmon, P. Meriaudeau, C. Mirodatos, Ind. Eng. Chem. Res. 33 (1994) 1460–1467.
[9] Q. J. Quarderer, G. A. Cochram, US patent WO84/03696, 1984.
[10] S. F. Zaman, K. J. Smith, Appl Catal. A: Gen. 378 (2010) 59–68.
[11] S. F. Zaman, K. J. Smith, Catal. Today 171 (2011) 266–74.
[12] M. Xiang, D. Li, H. Xiao, J. Zhang, H. Qi, W. Li, Fuel 87 (2008) 599–603.
[13] J.S.J. Hargreaves, Coord. Chem. Rev. 257 (2013) 2015–2031.
[14] D. Mckay, J.S.J. Hargreaves, J.L. Rico, J.L. Rivera, X.-L. Sun, J. Solid State Chem. 181 (2008) 325–333.
[15] A. M. Alexander, J. S. J. Hargreaves, Chem. Soc. Rev. 39 (2010) 4388–4401.
[16] S. T. Oyama, Catal. Today 15 (1992) 179–200.
[17] M. Nagai, Appl. Catal. A: Gen. 322 (2007)178–190.
[18] J.G. Chen, Chem. Rev. 96 (1996) 1477–1498.
[19] M. E. Eberhart, J. M. MacLaren "The chemistry of transition metal carbides and nitrides" S.T. Oyama Ed., Champman & Hall, New York, 1996, p 107.
[20] S. F. Zaman, Bul. Chem. Commun. 47 (2015) 125–132.
[21] N. Arumugam, thesis titled "New ternary alkali oxides and quaternary alkali oxy-nitrides of molybdenum and tungsten" Chapter 5, p 88.
[22] Z. Wei, Q. Xin, P. Grange, B. Delmon, J. Catal. 168 (1997) 176–182.
[23] R. Kojima, K.-I. Aika, Appl. Catal. A: Gen. 219 (2001) 141–147.
[24] C.H. Jaggers, J. N. Michaels, A. M. Stacy, Chem. Mater. 2 (1990) 150–157.
[25] M. Nagai, Y. Goto, A. Miyata, M. Kiyoshi, K. Hada, K. Oshikawa, S. Omi, J. Catal. 182 (1999) 292–301.
[26] K.S.W. Sing, D.H. Everett, R.A.W. Haul, L. Moscou, R.A. Pierotti, J. Rouquerol, T. Siemieniewska, Pure Appl. Chem. 57 (1985) 603–619.
[27] B. Ibeh, S. Zhang, J. M. Hill, Appl. Catal. A: Gen. 368 (2009) 127–131.
[28] V. M. L. Whiffen, K. J. Smith, S. K. Straus, Appl. Catal. A: Gen. 419–420 (2012) 111–125.

[29] S. Podila, S. F. Zaman, H. Driss, Y. A. Alhamed, A. Al-Zahrani, L. A. Petrov, Catal. Sci. Technol. 6 (2016) 1496–1506.
[30] R. Andersson, M. Boutonnet, S. Jaras, Appl. Catal. A: Gen. 417–418 (2012) 119–128.
[31] E.T. Liakakou, E. Heracleous, Catal. Sci Technol. 6 (2016) 1106–1119.
[32] J. Sangster, J. Phase Equilib. Diff. 34 (2013) 43–55.
[33] J. M. Moggia, V. G. Milt, M. A. Ulla, L. M. Cornaglia, Surf. Interface Anal. 35 (2003) 216–225.
[34] M.E. Gálvez, S. Ascaso, P. Stelmachowski, P. Legutko, A. Kotarba, R. Moliner, M.J. Lázaro, Appl. Catal. B: Environ. 152–153 (2014) 88–98.
[35] K. Hada , M. Nagai , S. Omi, J. Phys. Chem. B 105 (2001) 4084–4093.
[36] T. Kawai, K. Kunimori, T. Kondow, T. Onishi, K. Tamaru, Phy. Rev. Lett. 33 (1974) 533–536.
[37] C. L. Bulla, T. Kawashima, P. F. McMillan, D. Machon , O. Shebanova , D. Daisenberger, E. Soignard, E. T-. Muromachi, L. C. Chapon, J. Solid State Chem. 179 (2006) 1762–1767.
[38] A.Y. Ganin, L. Kienle, G.V. Vajenine, Electro Chemical Society Proceedings, Vol 2005-09, p 452–453.
[39] S. Yang, C. Li, J. Xu, Q. Xin, J. Phys. Chem. B 102 (1998) 6986–6993.
[40] J. A. Schaidle, L. T. Thompson, J. Catal. 329 (2015) 325–334.
[41] J. S. Lee, K. H. Lee, J.Y. Lee, J. Phys. Chem. 96 (1992) 362–366.
[42] V. P. Santos, B. van der Linden, A. Chojecki, G. Budroni, S. Corthals, H. Shibata, G. R. Meima, F. Kapteijn, M. Makkee, J. Gascon, ACS Catal. 3 (2013) 1634–1637.
[43] J. M. Christensen, L. D. L. Duchstein, J. B. Wagner, P. A. Jensen, B. Temel, A. D. Jensen, Ind. Eng. Chem. Res. 51 (2012) 4161–4172.
[44] X. Xiaoding, E. B. M. Doesburg J. J. F. Scholten, Catal. Today 2 (1987) 125–170.
[45] N. T-.Thao, H. M. Z-. Niaki, H. Alamdari, S. Kaliaguine, J. Catal. 245 (2007) 348–357.
[46] M. Saito, R.B. Anderson, J. Catal. 63 (1980) 438–446.
[47] T. Ahmad, K. Saba, Z. Zahra, T. Somayeh, A. Hamideh, B. Mokhtar, Iran. J. Chem. Eng 32 (2013) 21-29.
[48] P.L. Spath, D.C. Dayton. "Preliminary Screening -Technical and Economic Assessment of Synthesis Gas to Fuels and Chemicals with Emphasis on the Potential for Biomass-Derived Syngas", NREL/TP510-34929,December, 2003, p. 95.
[49] V. R. Surisetty, A. K. Dalai, J. Kozinski, Appl. Catal. A: Gen. 404 (2011) 1–11.
[50] J. M. Christensen, P. A. Jensen, N. C. Schiødt, A. D. Jensen, ChemCatChem. 2 (2010) 523–526.
[51] M. Jiang, G. -Z. Bian, Y. -L. Fu, J. Catal. 146 (1994) 144–154.

Table 1: BET, XRF, TEM and CO-TPD data for Mo_2N and K-Mo_2N catalysts

Catalyst	BET SA m^2/g	Pore volume cc/g	Nominal K wt.%	XRF K wt.%	EDS K wt.% [b]	Average TEM Mo_2N particle size (nm)
Mo_2N	110	0.071	-	-	-	7
0.45K-Mo_2N	10	0.015	1	0.45	-	-
1.3K-Mo_2N	8	0.013	5	1.3 (1.2)[a]	0.5	8
3K-Mo_2N	7	0.012	10	3 (2.9) [a]	0.2	10
6.2K-Mo_2N	6	0.013	15	6.2 (6.1) [a]	0.1	6

[a] spent catalyst

[b] Approximate K content present in the cubic γ-Mo_2N matrix estimated using parallel beam (supplementary image S1b)

Table 2: XPS data for Mo_2N and K-Mo_2N catalysts

Catalyst	**Mo distribution at. %**					**Surface ratio**	
	Mo^0	Mo^{+2}	Mo^{3+}	Mo^{4+}	Mo^{6+}	$K/(Mo^{2+}+Mo^{3+})$	$N/(Mo^{2+}+Mo^{3+})$
Mo_2N	-	10	3	9	10	-	1.0
Mo_2N spent	-	9	2	10	11	-	0.95
0.45K-Mo_2N	-	8	9	8	8	0.008	0.6
1.3K-Mo_2N	-	15	6	7	7	0.06	0.4
1.3K-Mo2N spent	-	14	6	8	8	0.058	0.39
3K-Mo_2N	-	8	10	8	9	0.18	0.55
6.2K-Mo_2N	3	5	-	12	10	1.9	1.0

Figure captions

Fig. 1A: XRD pattern for calcined precursors with molybdenum, citric acid and potassium (a) Mo-CA (b) 1K-Mo-CA (c) 5K-Mo-CA (d) 10K-Mo-CA (e) 15K-Mo-CA; **1B:** XRD pattern for passivated samples.

Fig. 2: (a) BET isotherms for passivated samples (b) pore size distribution of passivated samples

Fig.3A: K 2p; **3B:** Mo 3d and **3C:** N KLL Auger spectra of
(a) 1.3K-Mo_2N (b) 3K-Mo_2N (c) 6.2K-Mo_2N

Fig.4: TEM/HR-TEM, SAED images (a) 1.3K-Mo_2N TEM (b) 1.3K-Mo_2N HR-TEM/SAED (c) 3K-Mo_2N TEM (d) 6.2K-Mo_2N HR-TEM (e) HR-TEM of Mo_2N matrix in 3K-Mo_2N (f) HR-TEM of Mo_2N & MoN matrix of 6.2K-Mo_2N sample

Fig.5: CO-TPD-mass analysis of passivated samples

Fig.6: DRIFTs analysis on (a) Mo_2N (b) 1.3K-Mo_2N at 300 ^oC and 5MPa.

Fig.7: (a) CO hydrogenation activity with respect to potassium loading at reaction temperature 275-325 ^oC, 7MPa and GHSV 60000 h^{-1} (b) alcohol and other liquid product (butanol, acetone and ethyl acetate) distribution with respect to potassium loading at 300 and 325 ^oC.

Fig.8: (a) Influence of GHSV on CO hydrogenation activity of 1.3K-Mo_2N at 300 ^oC and 7 MPa (b) influence of K/$Mo^{\delta+}$ surface ration on C_2^+ oxygenates selectivity at different potassium loadings, 300 ^oC and 7 MPa.

Fig.9: Time on stream results on Mo_2N and 1.3K-Mo_2N catalysts at 300^oC, 7MPa and 60,000 h^{-1}.

Fig.10: XRD pattern of passivated, reduced, spent 1.3K-Mo_2N catalyst.

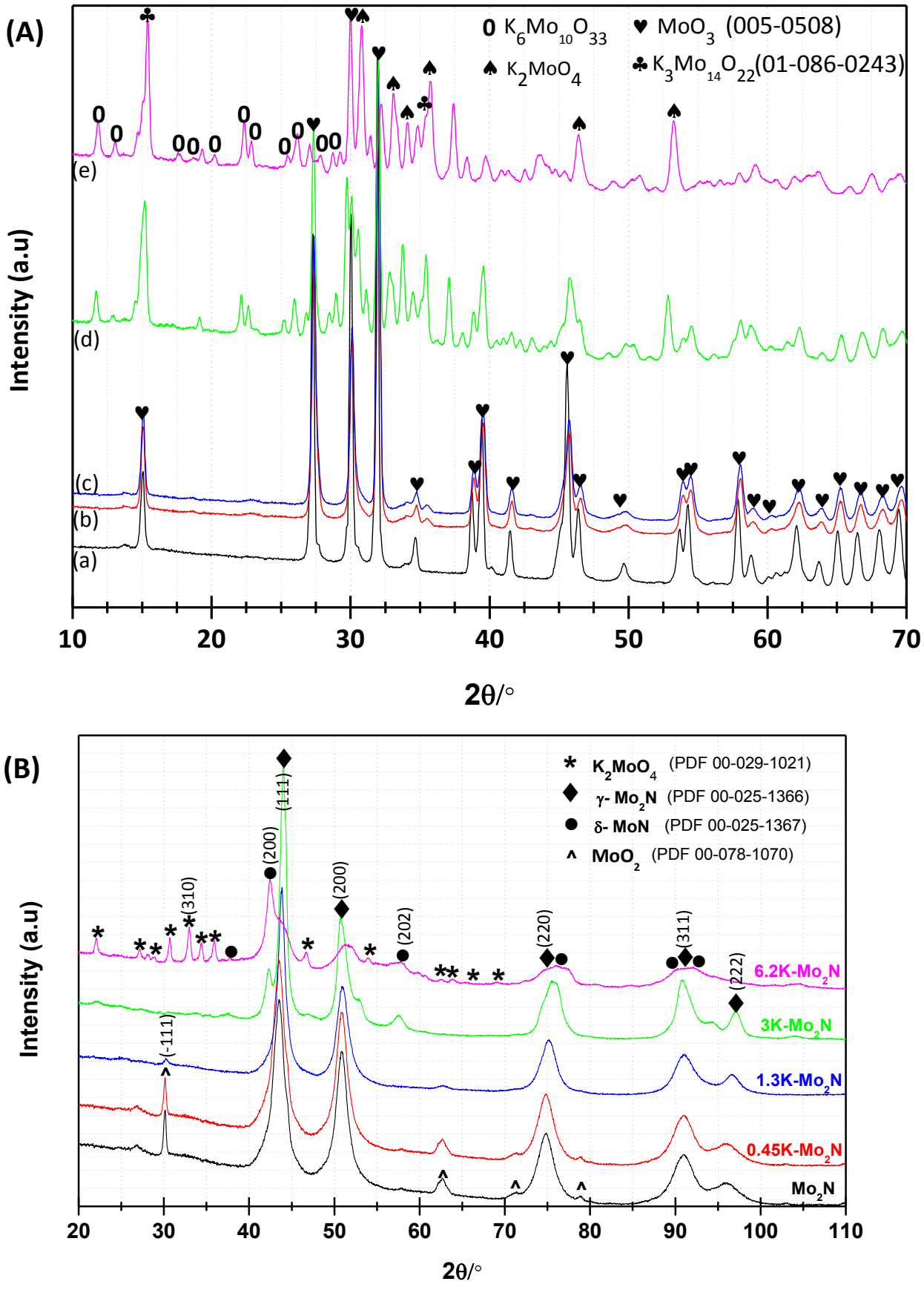

Fig. 1

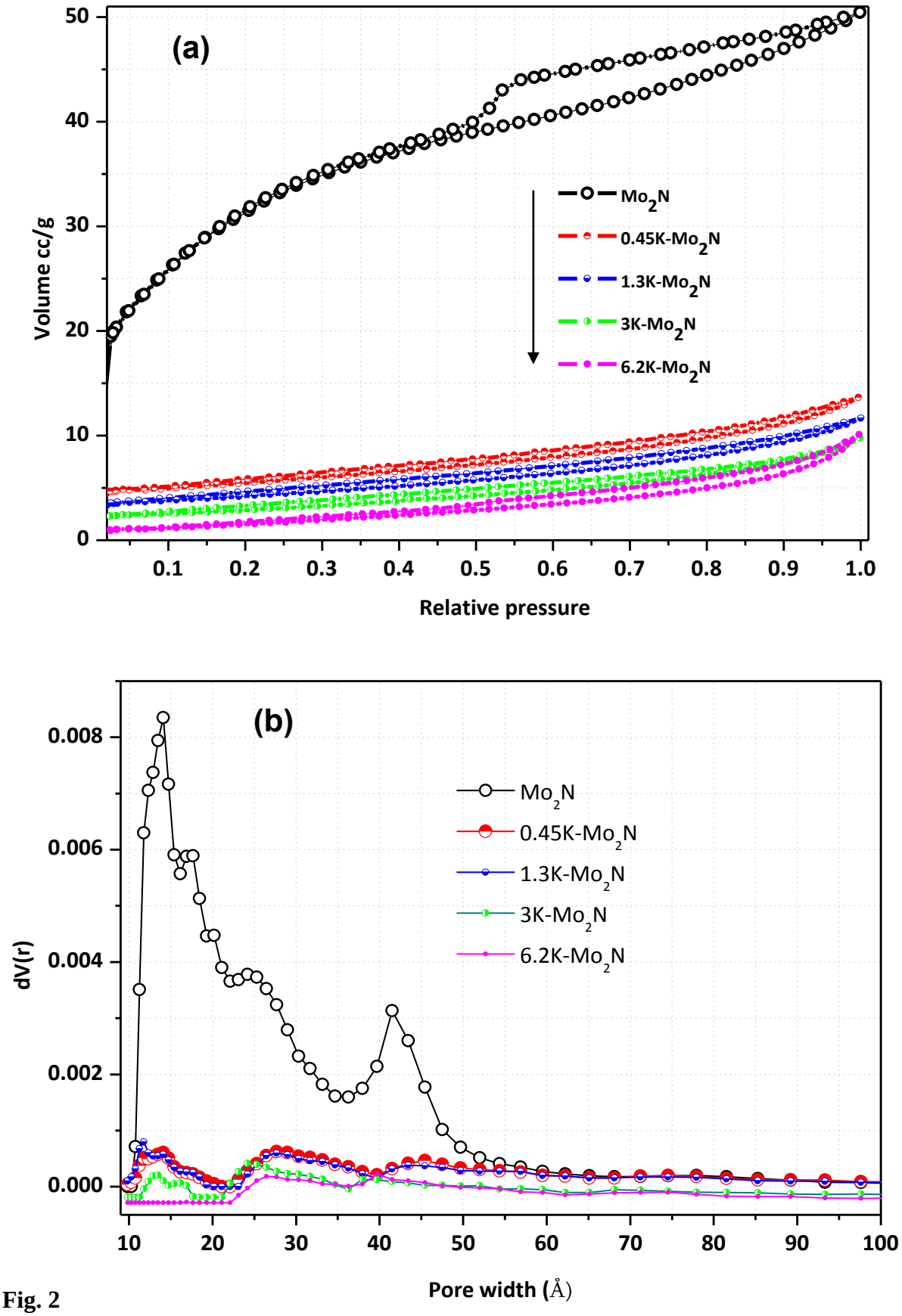

Fig. 2

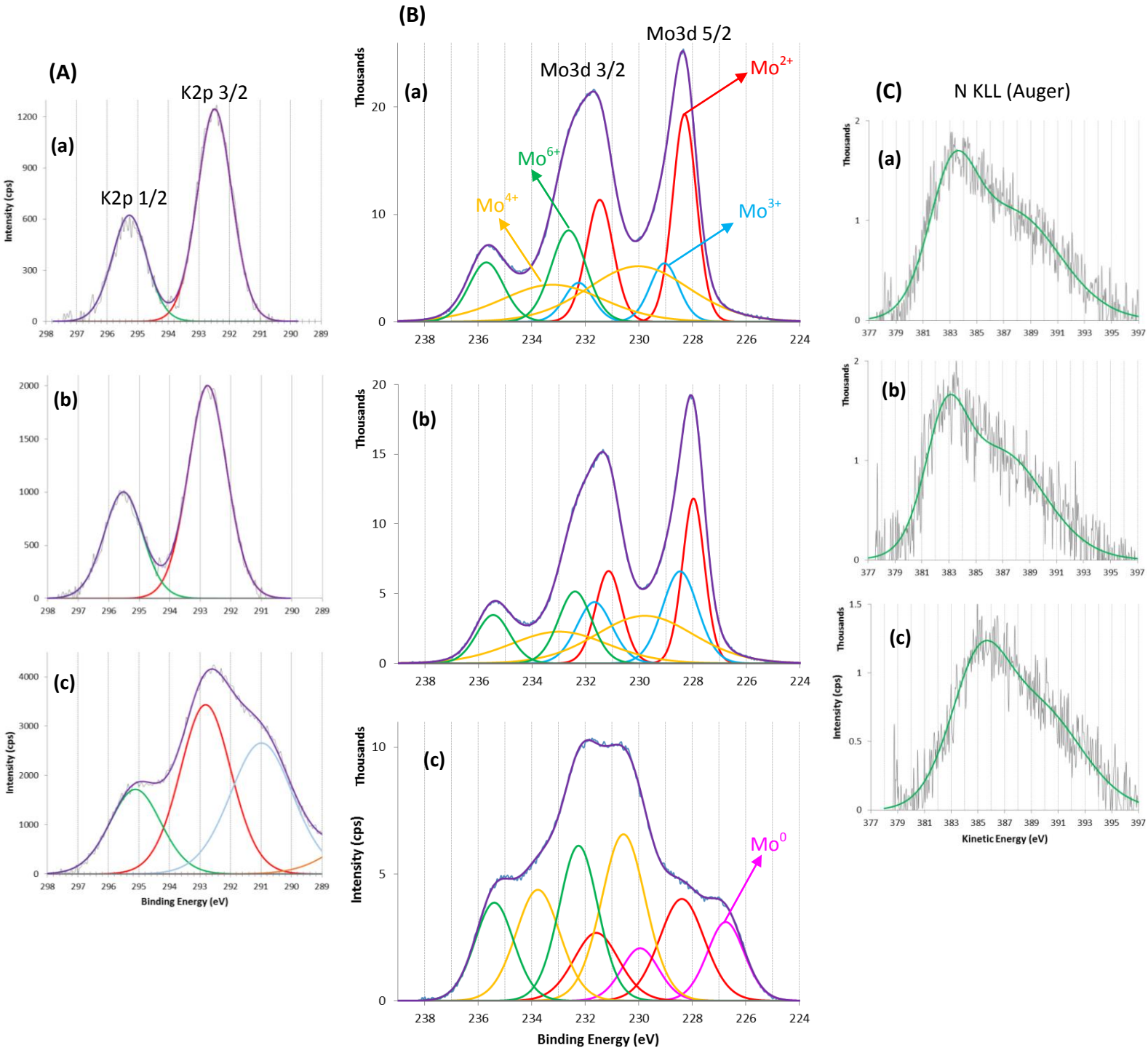

Fig. 3

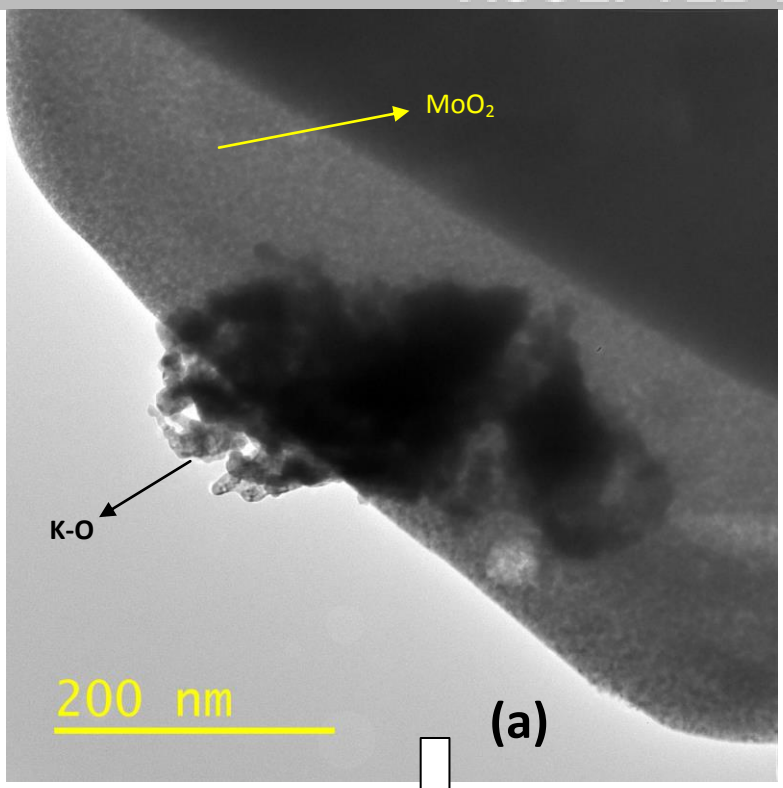

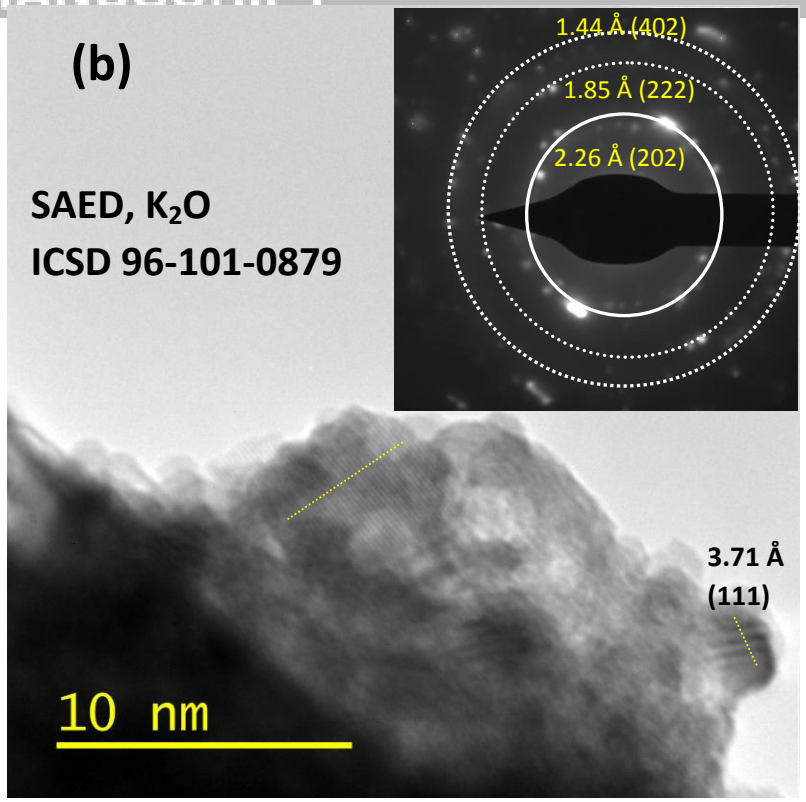

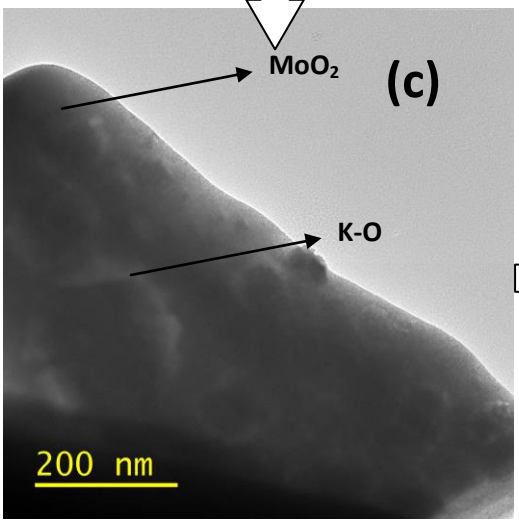

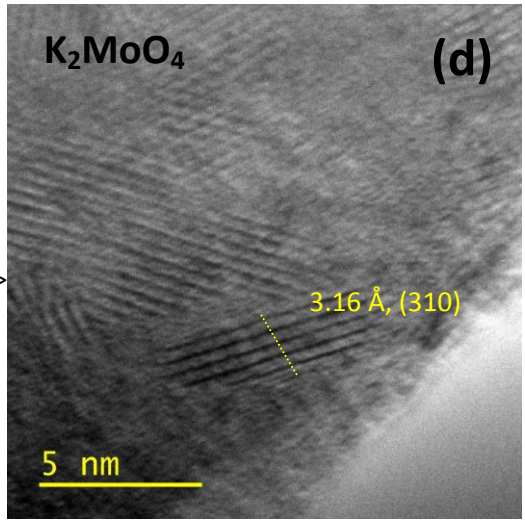

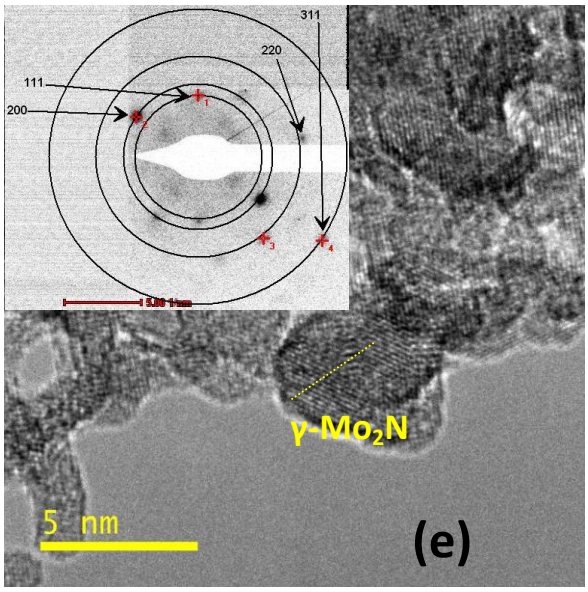

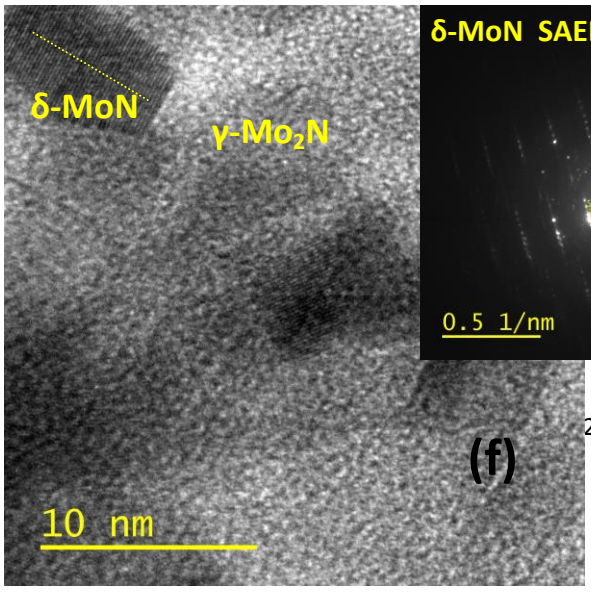

Fig. 4

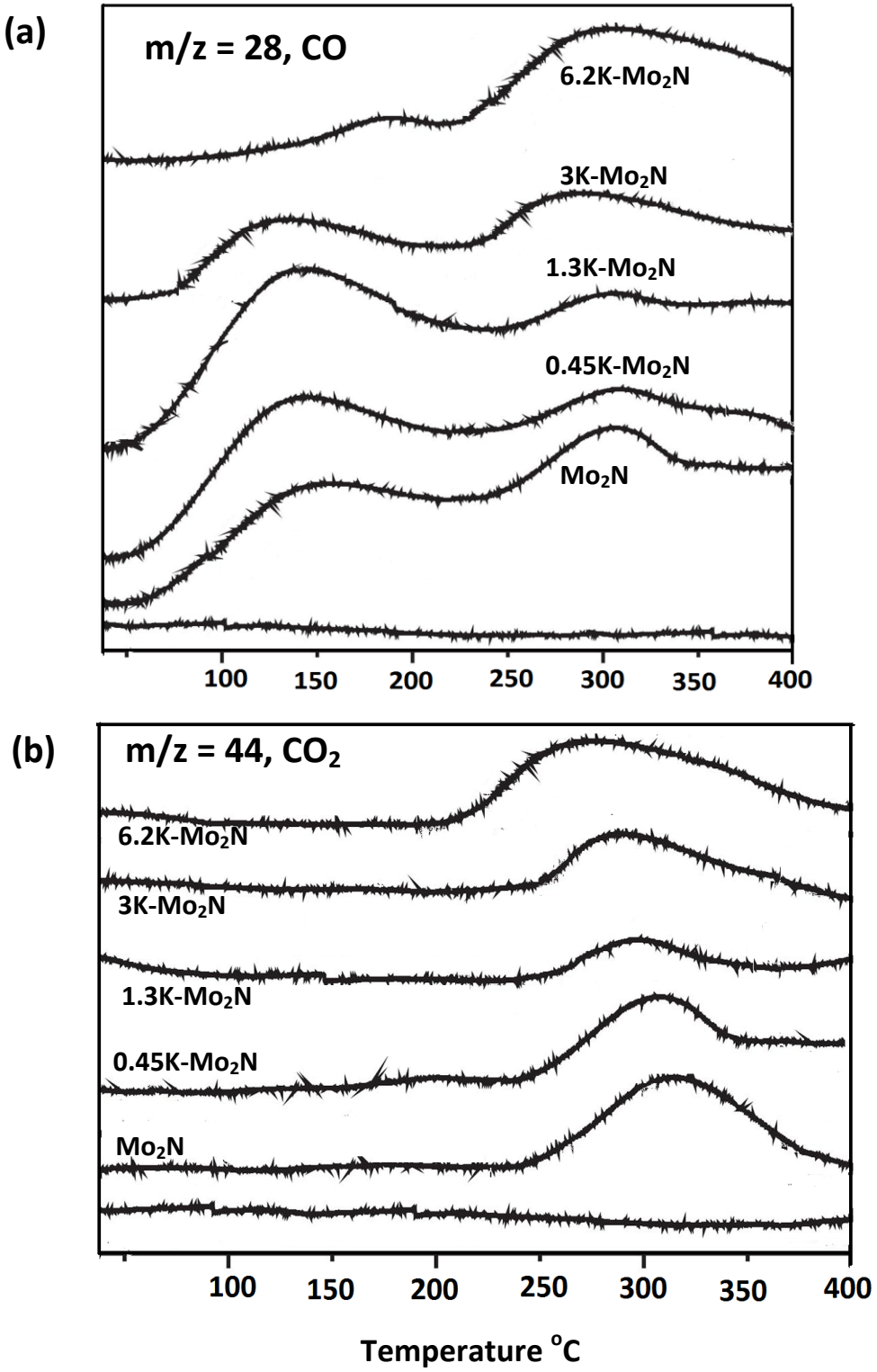

Fig. 5

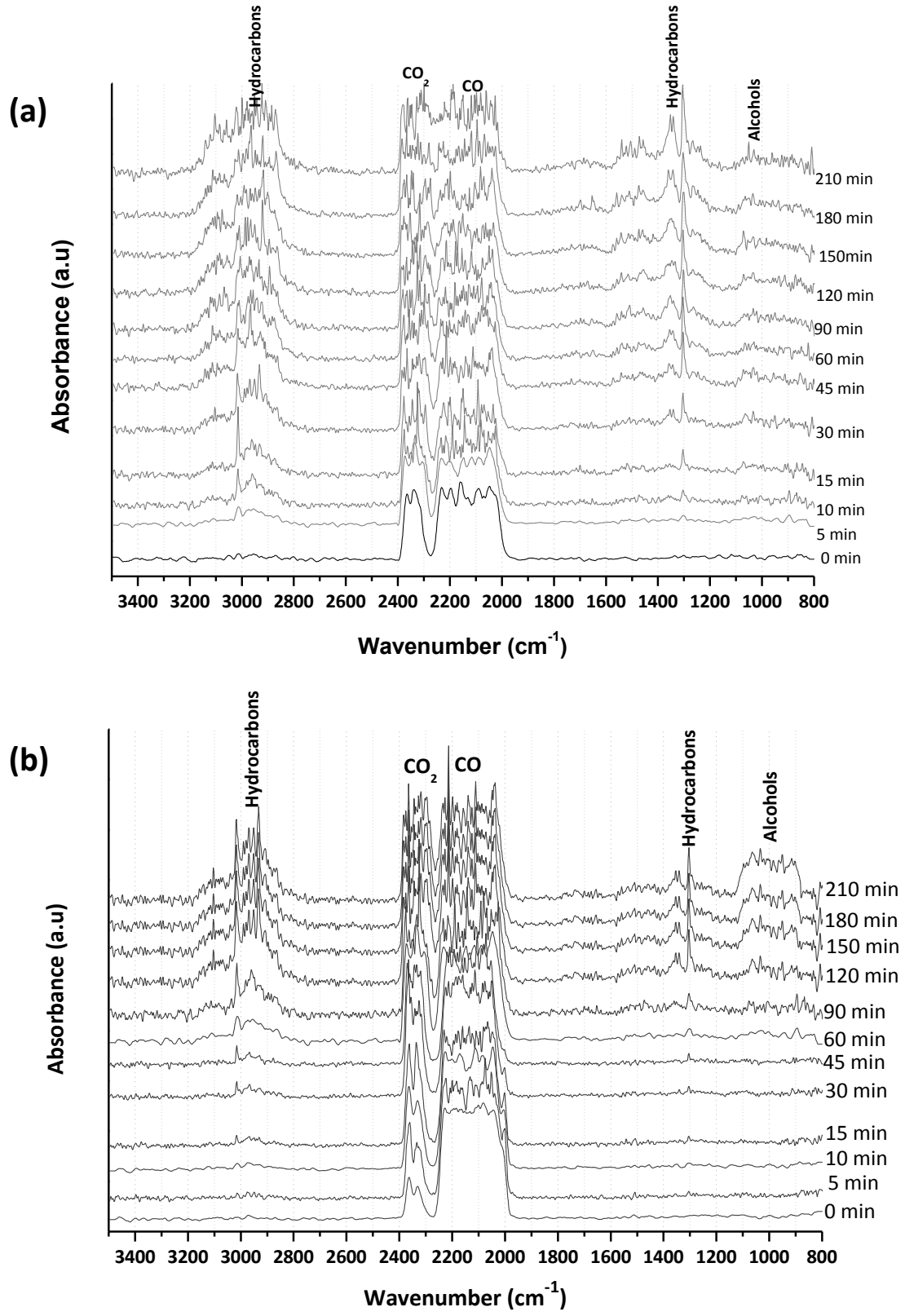

Fig. 6

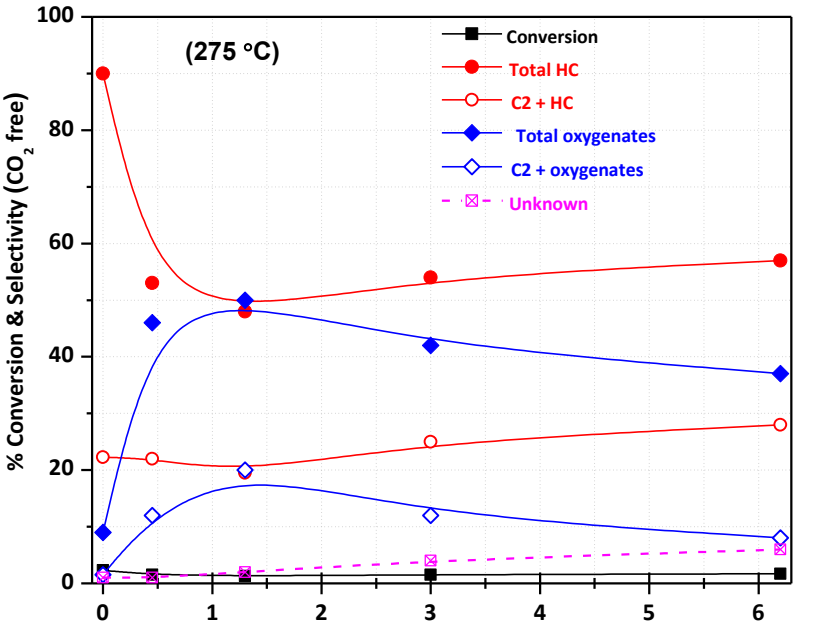

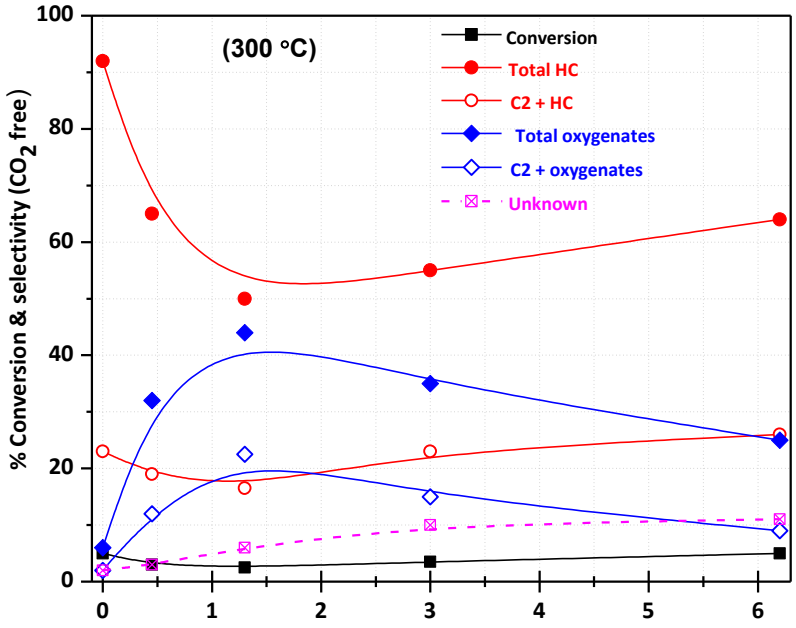

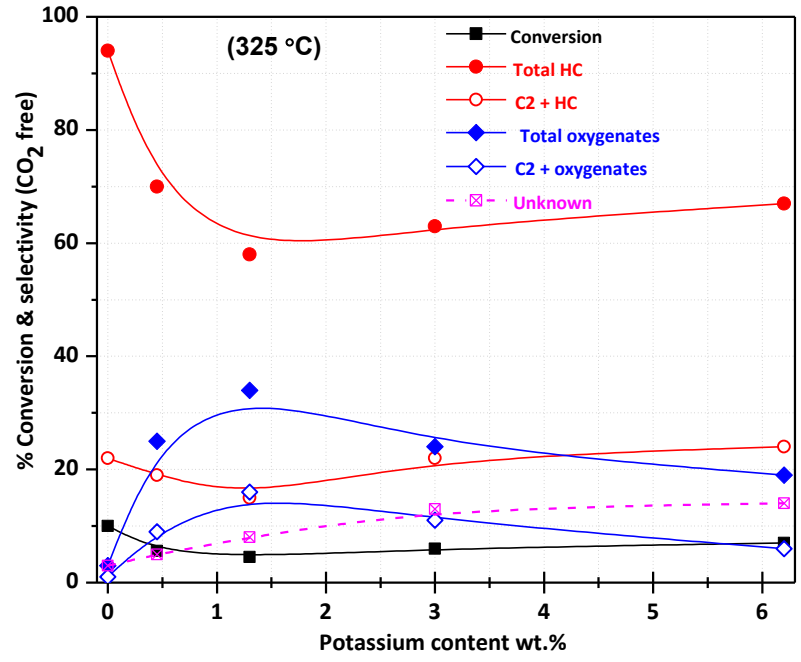

Fig. 7a

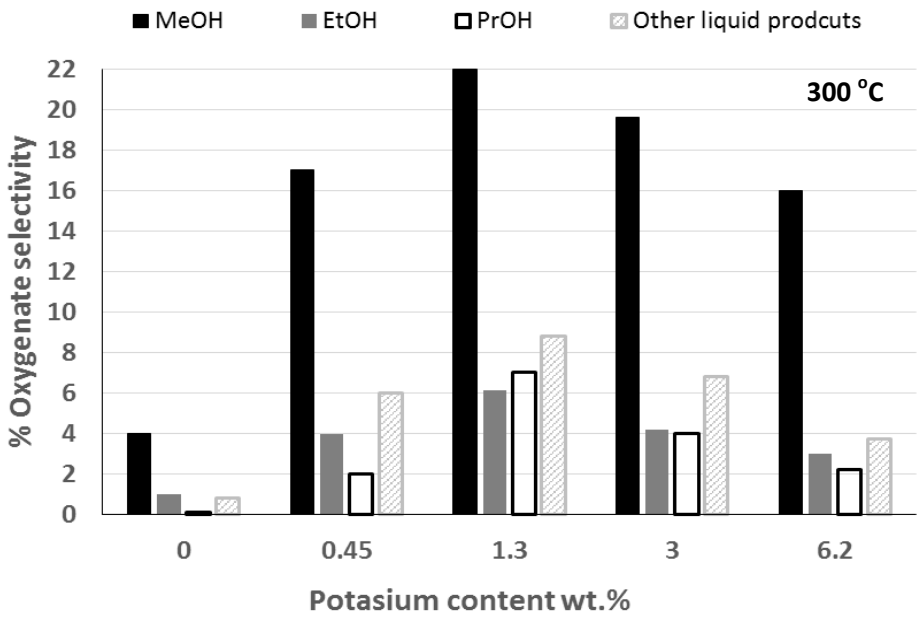

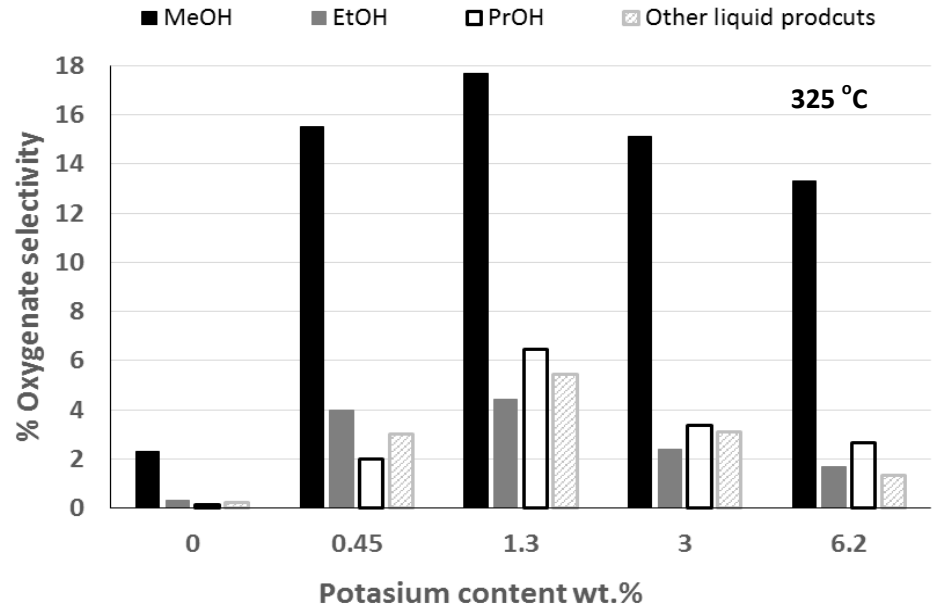

Fig. 7b

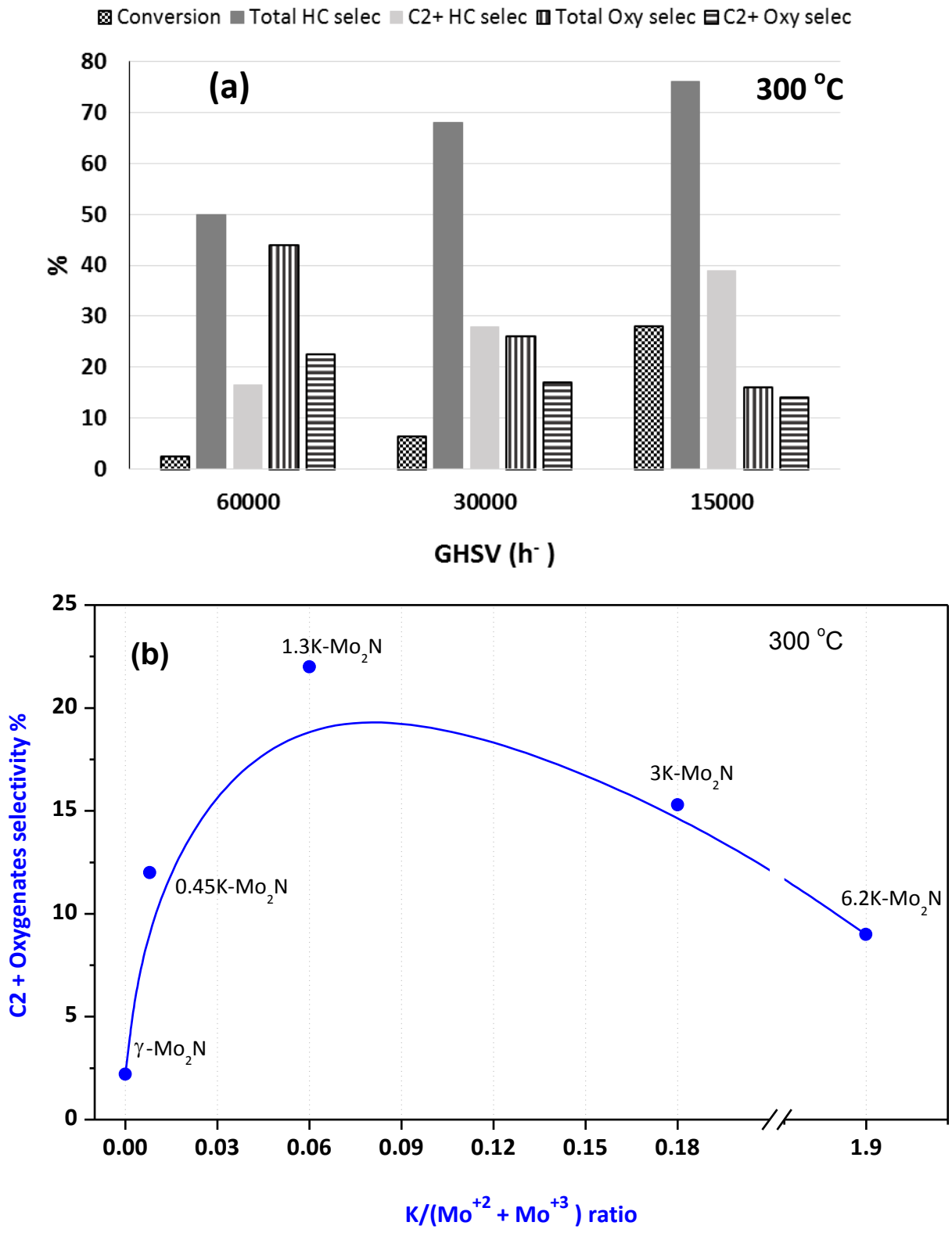

Fig .8

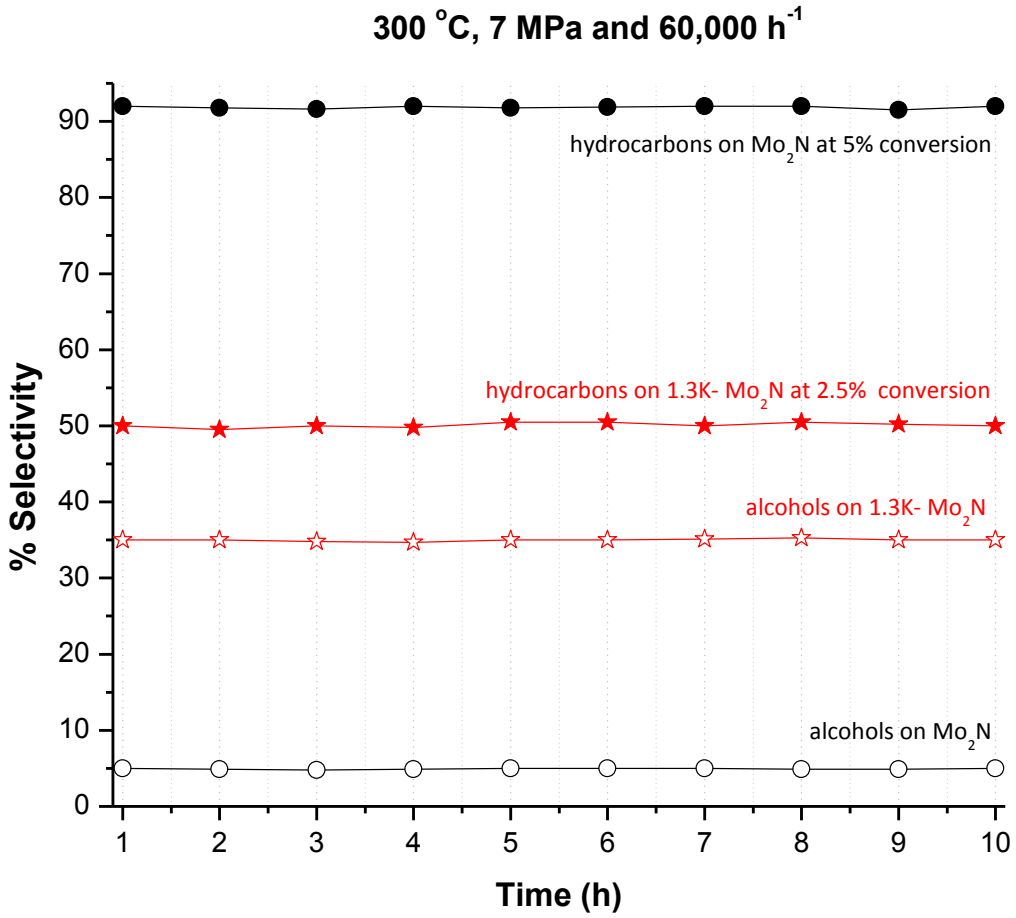

Fig. 9

Hydrogenation on Mo_2N

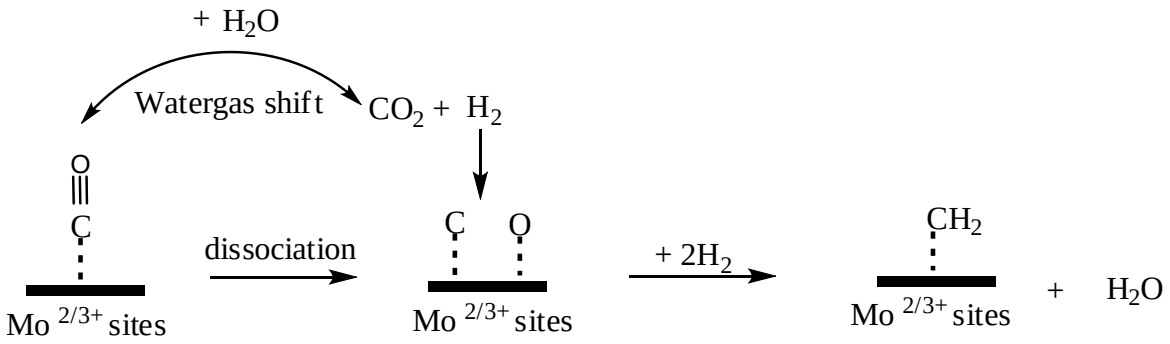

Alcohols on K promoted Mo_2N

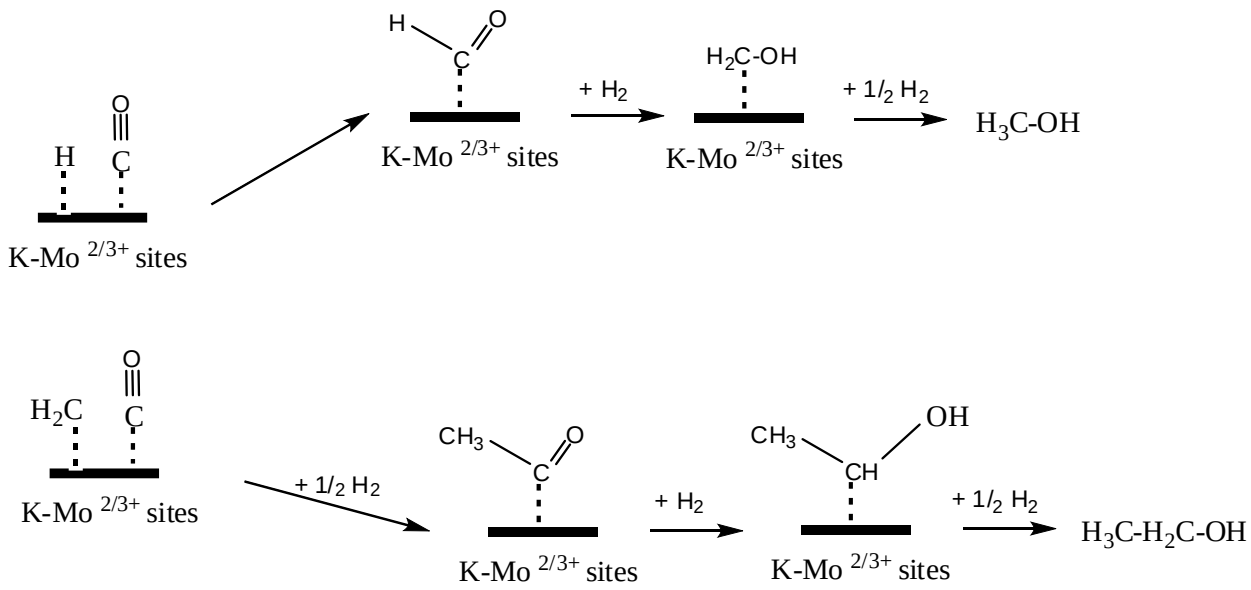

Scheme 1: plausible CO hydrogenation reaction pathways on Mo_2N and K-Mo_2N catalysts

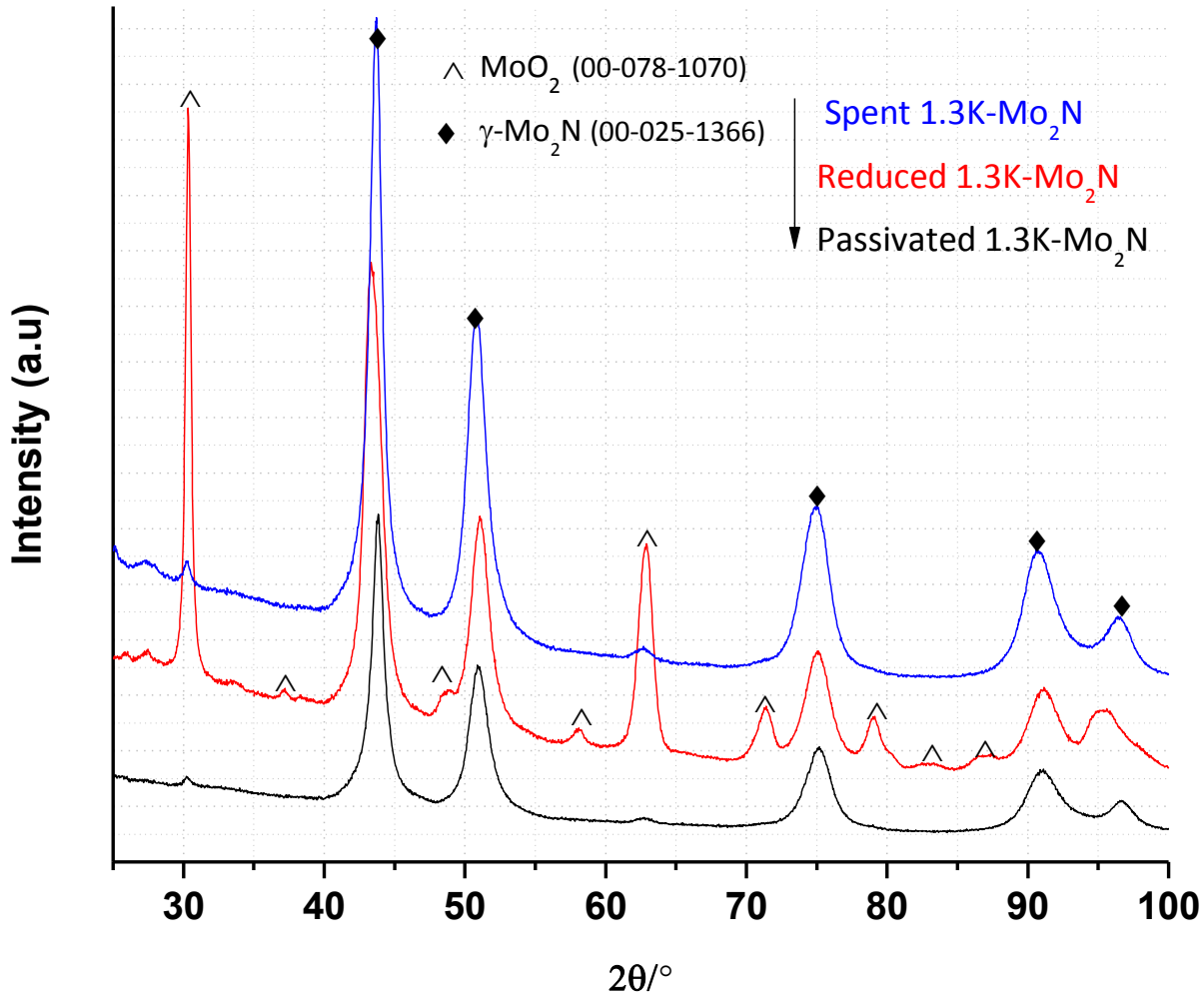

Fig. 10